iScience

CellPress
OPEN ACCESS

Article

RGS12 Is a Novel Critical NF-κB Activator in Inflammatory Arthritis

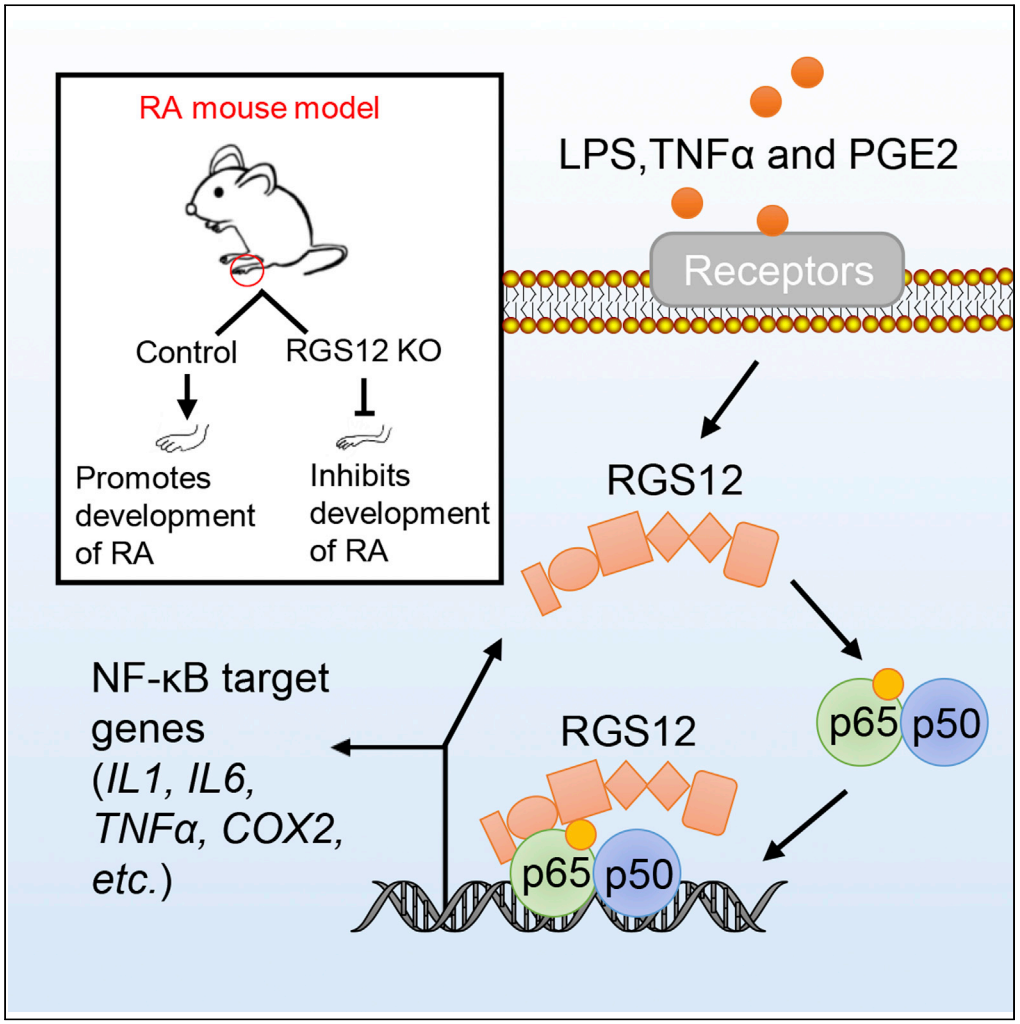

Gongsheng Yuan, Shuting Yang, Andrew Ng, Chuanyun Fu, Merry Jo Oursler, Lianping Xing, Shuying Yang

shuyingy@upenn.edu

HIGHLIGHTS

RGS12 regulates inflammation through activating an RGS12-NF-κB positive feedback loop

RGS12 activates NF-κB nuclear translocation and phosphorylation

PTB domain of RGS12 promotes the association of RGS12 and NF-κB

COX2 enhances nuclear translocation of RGS12/NF-κB in inflammatory conditions

Yuan et al., iScience *23*, 101172
June 26, 2020
https://doi.org/10.1016/j.isci.2020.101172

iScience

CellPress
OPEN ACCESS

Article

RGS12 Is a Novel Critical NF-κB Activator in Inflammatory Arthritis

Gongsheng Yuan,[1] Shuting Yang,[1] Andrew Ng,[2] Chuanyun Fu,[1] Merry Jo Oursler,[3] Lianping Xing,[4] and Shuying Yang[1,5,6,7,*]

SUMMARY

Rheumatoid arthritis (RA) is the most common inflammatory disease, which currently lacks effective treatment. Here, we discovered that the Regulator of G Protein Signaling 12 (RGS12) plays a key role in regulating inflammation. Transcriptional and protein analysis revealed that RGS12 was upregulated in human and mouse RA macrophages. Deletion of RGS12 in myeloid lineage or globally inhibits the development of collagen-induced arthritis including joint swelling and bone destruction. Mechanistically, RGS12 associates with NF-κB(p65) to activate its phosphorylation and nuclear translocation through PTB domain, and NF-κB(p65) regulates RGS12 expression in a transcriptional manner. The nuclear translocation ability of NF-κB(p65) and RGS12 can both be enhanced by cyclooxygenase-2 (COX2). Furthermore, ablation of RGS12 via RNA interference significantly blocks the inflammatory process *in vivo* and *in vitro*. These results demonstrate that RGS12 plays a critical role in the pathogenesis of inflammatory arthritis.

INTRODUCTION

Rheumatoid arthritis (RA) is the most common inflammatory disease with a marked expansion of the normally hypocellular synovium by infiltrating leukocytes, including synovial macrophages (SMs), which leads to the destruction of adjacent cartilage and bone (Smolen et al., 2016; Tang et al., 2011). Macrophages are one of the most abundant cell types in the RA synovium, and evidence indicates that macrophages are activated in RA and can directly drive the progression of RA (Choi et al., 2017). Macrophages are a major source of cytokines and chemokines, such as monocyte chemoattractant protein 1 (MCP1), granulocyte-macrophage-colony-stimulating factor (GM-CSF), tumor necrosis factor (TNF), and the interleukins (Sprague and Khalil, 2009). Enzyme cyclooxygenase-2 (COX2) produced from activated macrophages contributes to pain and swelling via promoting the production of inflammatory mediators such as prostaglandin E(2) (PGE2), which has been a major target of biological therapy (Bouta et al., 2018; Samad et al., 2001). Moreover, persistent activation of certain signaling pathways including NF-κB (Nuclear Factor kappa-light-chain-enhancer of activated B cells) and PI3K-AKT (Phosphoinositide 3-kinases-Protein kinase B) enhances resistance to cell apoptosis or cytokine withdrawal (Pope, 2002). Therefore, targeting macrophages is a potentially effective way to inhibit inflammatory arthritis.

NF-κB plays a critical role in inflammation or RA owing to its principal function in transcriptional regulation of inflammatory cytokines (Yao et al., 2009). NF-κB is activated by receptor molecules located in the cell membrane such as TNF receptor (TNFR) superfamily members, ligands of various cytokine receptors, as well as pattern-recognition receptors (PRRs) (Liu et al., 2017). Activation of canonical NF-κB, a dimer comprising NF-κB1 (p50) and RelA (p65), is triggered by the phosphorylation-induced degradation of IκB and followed by the transcriptional activation of target genes in the nucleus (Vallabhapurapu and Karin, 2009). The phosphorylation of the NF-κB subunits has a profound effect on cell functions, which controls the interactions with other factors such as MYBBP1a (MYB Binding Protein 1a) and CBP (CREB-binding protein) (Christian et al., 2016; Milanovic et al., 2014). Activation of NF-κB steadily increases numerous known genes including cytokines, chemokines, cellular ligands, and adhesion molecules, which contributes to RA development and progression (Sundaram et al., 2009; Yuan et al., 2019). Thus, inhibition of NF-κB signaling or related pathways may have a huge potential for the treatment of RA (Yamamoto and Gaynor, 2001).

The Regulator of G-protein signaling (RGS) protein family contains a conserved RGS domain, which is often accompanied by other signaling regulatory domains (Neubig and Siderovski, 2002). RGS proteins

[1]Department of Basic and Translational Sciences, School of Dental Medicine, University of Pennsylvania, Philadelphia, PA, USA

[2]Department of Oral Biology, School of Dental Medicine, University of Buffalo, State University of New York, Buffalo, NY, USA

[3]Department of Medicine, Endocrine Research Unit, Mayo Clinic, Rochester, MN, USA

[4]Department of Pathology and Laboratory Medicine, Center for Musculoskeletal Research, University of Rochester Medical Center, Rochester, NY, USA

[5]The Penn Center for Musculoskeletal Disorders, School of Medicine, University of Pennsylvania, Philadelphia, PA, USA

[6]Center for Innovation & Precision Dentistry, School of Dental Medicine, School of Engineering and Applied Sciences, University of Pennsylvania, Philadelphia, PA, USA

[7]Lead Contact

*Correspondence: shuyingy@upenn.edu

https://doi.org/10.1016/j.isci.2020.101172

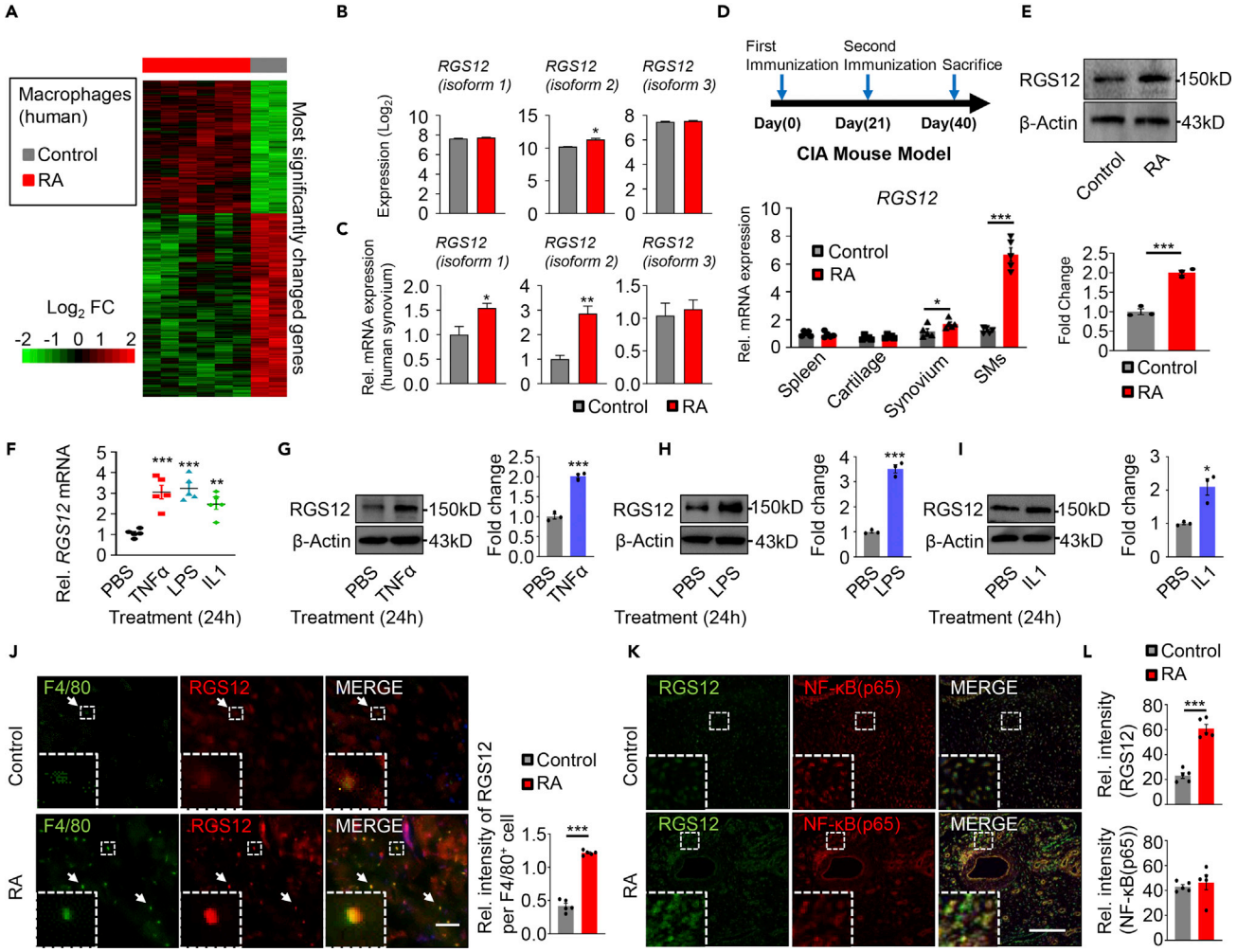

Figure 1. RGS12 Expression Is Upregulated in Inflammatory Arthritis

(A) Identification of a human gene signature (Database: GSE49604) consisting of 1,576 most changed mRNAs (FDR<0.05) in macrophages from RA synovial fluid (red box, n = 6) compared with healthy control macrophages (gray box, n = 2) differentiated from peripheral blood monocytes. Red and green denote increase and decrease in mRNA expression, respectively. Each line on the heatmap represents a gene/gene family (see also Figure S1 and Table S5).

(B) Bar graphs illustrating the expression of the different *RGS12* isoform genes (*isoforms 1–3*) associated with RA in human macrophages as described in Figure 1A (Control [gray] and RA [red]). Asterisks indicate significant differential expression (FDR<0.05).

(C) Real-time PCR showing altered expression of *RGS12 isoforms* in Control (gray) and RA synovium (red). Data are presented as the mean ± SEM. *p < 0.05, **p < 0.01 versus the control group (n = 5).

(D) Study design for induction of CIA (collagen-induced arthritis) in an animal model. WT (wild-type, C57/BL6) mice were immunized with chicken type II collagen on day 0 and boosted on day 21. All mice were sacrificed on day 40.

Quantification by real-time PCR of *RGS12* using total RNA isolated from spleen, cartilage, synovium, and SMs in Control (WT) and RA mice. Results are from five independent RNA preparations, analyzed by real-time PCR in triplicates with *GAPDH* as an internal control. Data are analyzed by unpaired t test, and asterisks on the graphs indicate p values of significance, *p < 0.05, ***p < 0.001, (n = 5).

(E) Western blot analysis of RGS12 expression in SMs from Control (WT) and RA mice on day 40 (top panel). Quantitation of RGS12 protein levels (bottom panel). The data are normalized to β-Actin. ***p < 0.001 versus the control group, (n = 3).

(F) *RGS12* mRNA expression was increased in TNF-α (10 ng/mL), LPS (1 μg/mL), and IL-1 (10 ng/mL)-induced BMMs for 24 h **p < 0.01, ***p < 0.001 versus the control group, (n = 5).

(G–I) Western blot analysis of RGS12 expression level in TNF-α (10 ng/mL) (G), LPS (1 μg/mL) (H), and IL-1 (10 ng/mL) (I)-treated BMMs for 24 h and statistical analysis of RGS12 in the indicated groups (n = 5). Data are presented as the mean ± SEM. *p < 0.05, ***p < 0.001 versus the control group.

(J) Double immunofluorescence labeling showing that RGS12 is expressed in F4/80$^+$ macrophages in synovial tissue. Merged image showing RGS12 and F4/80 labeling. Scale bar, 100 μm. Representative individual and overlaid images are shown. Quantitative results of Integrated Optical Density (IOD) of RGS12 per F4/80$^+$ cell in the control and RA groups. ***p < 0.001, (n = 5).

Figure 1. *Continued*

(K) Immunofluorescence showing that RGS12 and NF-κB(p65) show co-localization in human synovial tissue. Scale bar, 200 μm. Representative individual and overlaid images are shown.

(L) Quantitative results of IOD in sections of RGS12 and NF-κB(p65) in the control and RA groups as shown in (K). Note that RGS12 significantly increases in RA but not the total NF-κB(p65). ***$p < 0.001$ ($n = 5$).

accelerate the deactivation of G proteins to turn off GPCR signaling (Neubig and Siderovski, 2002). Recently, RGS proteins were found to play important roles in both innate and adaptive immune responses (Druey, 2017). RGS1 regulates myeloid cell accumulation in atherosclerosis through altered chemokine signaling (Patel et al., 2015). RGS10 expression is inhibited in activated microglia through altered histone deacetylase activity (Alqinyah et al., 2017). Therefore, RGS proteins may become important and new drug targets for the treatment of immune and inflammatory diseases.

Regulator of G Protein Signaling 12 (RGS12) was first found as the largest protein in the RGS family (Snow et al., 1997). Further studies found that RGS12 is located in both the cytosol and the nucleus (Willard et al., 2007) and contains an N-terminal PDZ (PSD-95, disc-large, zo-1) domain, PTB (phosphotyrosine binding) domain, RGS domain, tandem RAS-binding domain (RBD), and a GoLoco (Gαi/o-Loco) interaction motif, which play important roles through binding different proteins (Snow et al., 1998; Ponting, 1999; Siderovski et al., 1999; Kimple et al., 2001). RGS12 is involved in multiple signaling pathways, including G protein-coupled receptors (GPCRs) (Kimple et al., 2001), receptor tyrosine kinases (RTKs) (Willard et al., 2007), Ras GTPases (Snow et al., 1998; Willard et al., 2007), and MEK1/2-ERK1/2 coordinated signaling (Huang et al., 2016).

RGS12 has been reported to be closely associated with some diseases (Huang et al., 2016; Qi et al., 2017). The loss of RGS12 leads to the development of pathological cardiac hypertrophy and heart failure through MEK1/2-ERK1/2 signaling pathway (Huang et al., 2016). Our laboratory found that deletion of RGS12 in myeloid lineage caused mouse growth retardation with increased bone mass (Yang et al., 2013; Yuan et al., 2015). Notably, by analyzing *FCGR2A* functionally related genes in response to TNF-α antibody (adalimumab) treatment through microarray-based studies, Avila-Pedretti et al. found that there was a significant association between *FCGR2A* and the response to adalimumab, and *DHX32* and *RGS12* were the most consistently correlated genes with *FCGR2A* expression in RA synovial fluid macrophages (Avila-Pedretti et al., 2015). However, the function and mechanism of RGS12 involved in RA have not yet been uncovered.

In this study, we investigated the role of RGS12 in the regulation of RA progression by creating and analyzing the RGS12 global and macrophage lineage conditional knockout (*CMVCre*$^{+}$*;RGS12*$^{fl/fl}$ and *LysMCre*$^{+}$*;RGS12*$^{fl/fl}$) mouse models. Our findings demonstrated that RGS12 is essential for NF-κB inflammatory signaling transduction and thereby plays a key role in the progression of RA.

RESULTS

RGS12 Expression Is Upregulated in Inflammatory Arthritis

RA is characterized with an increased number of SMs. By using NIH GEO database (GSE49604) to analyze the human global expression of genes in synovial fluid macrophages from patients with RA and healthy macrophages differentiated from peripheral blood monocytes (You et al., 2014), we identified 1,576 genes that are mostly changed (with an FDR of less than 0.05 between RA SMs and healthy control macrophages) (Figure 1A and Table S5). Subsequently, we identified upregulated and downregulated RGS family genes (Figure S1). We found that *RGS1* and *RGS12 (isoform 2)* were significantly upregulated, whereas *RGS2* and *RGS14* were significantly downregulated (Figure S1). Notably, *RGS12* gene has three isoforms in human, and the expression levels of *isoform 2* significantly increase during RA (Figure 1B). We then performed real-time PCR from human synovial tissue to confirm the GEO data, discovering that *RGS12 isoform 1* and *isoform 2* showed a significant change in human RA synovial tissue (Figure 1C). However, no significant changes were found in *RGS12 isoform 3*. Interestingly, among the three *isoforms, RGS12 isoform 2 is the longest transcript with PDZ, PTB, and specialized C terminus,* which showed the most severe increase in expression in human RA synovial tissue (Figure 1C). We then tested the expression level of the longest *RGS12* gene in a mouse model of chicken type II collagen-induced arthritis (CIA), which shows the main features of RA (Figure 1D). We found that *RGS12* mRNA expression level significantly increased in synovium and SMs of CIA mice when compared with the control mice (Figure 1D). Consistently, RGS12 protein level also increased in SMs by immunoblotting assay (Figure 1E). To further explore the inflammatory mechanisms of RGS12 *in vitro*, we tested the expression of RGS12 in response to inflammatory stimuli including

TNF-α, LPS, and IL-1 and found RGS12 mRNA (Figure 1F) and protein expressions were upregulated with TNF-α (Figure 1G), LPS (Figure 1H), and IL1 (Figure 1I) stimulation in RAW264.7 cells.

To explore the expression pattern and role of RGS12 in human RA, we performed immunofluorescence staining in human RA synovial tissue and found that RGS12 expression was significantly enhanced in RA SMs as compared with the healthy synovial tissue (Figure 1J). NF-κB, as a central inflammatory regulator, plays a key role in the orchestration of the multifaceted inflammatory response, not only in the pro-inflammatory phase but also in the regulation of the resolution of inflammation (Gasparini and Feldmann, 2012). Interestingly, our results showed that RGS12 and NF-κB(p65) co-localized in synovium of both non-RA and RA patients (Figure 1K), and the RGS12 expression level was significantly increased in the synovium of patients with RA compared with the control (Figure 1L).

Deletion of RGS12 Inhibits the Spontaneous Development of Inflammatory Arthritis in CIA Mice

To examine the role of RGS12 during inflammatory arthritis development *in vivo*, we created *RGS12* global knockout (*CMVCre*$^{+}$;*RGS12*$^{fl/fl}$) and the conditional knockout of RGS12 in myeloid cell-line (*LysMCre*$^{+}$;*RGS12*$^{fl/fl}$) mouse models and investigated the clinical and histopathological features of these RGS12-deficient mice in CIA development (Figures 2A and S2). Both *CMVCre*$^{+}$;*RGS12*$^{fl/fl}$ and *LysMCre*$^{+}$;*RGS12*$^{fl/fl}$ developed much less severe joint swelling and bone destruction compared with the control mice (Figures 2B and 2C). Additionally, the arthritis severity score (Figure 2D), the paw thickness (Figure 2E), and the incidence of arthritis were also significantly decreased in RGS12-deficient mice compared with the control (Figure 2F). Histological and quantitative analysis of H&E-stained joint sections of whole ankles demonstrated a significant decrease in synovitis (*CMVCre*$^{+}$;*RGS12*$^{fl/fl}$, 62%; *LysMCre*$^{+}$;*RGS12*$^{fl/fl}$, 70%, $p < 0.001$), pannus formation (*CMVCre*$^{+}$;*RGS12*$^{fl/fl}$, 65%; *LysMCre*$^{+}$;*RGS12*$^{fl/fl}$, 79%, $p < 0.001$), and destruction of bone and cartilage (*CMVCre*$^{+}$;*RGS12*$^{fl/fl}$, 73%; *LysMCre*$^{+}$;*RGS12*$^{fl/fl}$, 77%, $p < 0.001$) in RGS12-deficient mice compared with those in control mice (Figures 2G and 2H). Hallmark genes of arthritis, such as *TNFα*, *IL6*, *COX2* (Figure 2I) in SMs, and the COX2 enzymatic product PGE2 in serum were decreased in both *CMVCre*$^{+}$;*RGS12*$^{fl/fl}$ and *LysMCre*$^{+}$;*RGS12*$^{fl/fl}$ mice with RA on day 40 after immunization (Figure 2J).

RGS12 Is Essential for the Phosphorylation of NF-κB(p65) and IκBα

To understand the mechanism of RGS12 in RA, we first identify the subcellular localization of RGS12 by immunofluorescence staining in RAW264.7 cells (Figure 3A). Our data showed that RGS12 was located mainly in the cytoplasm in non-inflammatory condition (Figure 3A). TNF-α or LPS stimulation increased the expression level and nuclear translocation of RGS12 (Figures 3A–3C) in a dose-dependent manner. TNF-α is one of the most potent physiological inducers of the nuclear transcription factor NF-κB(p65). It has been proved that RGS12 is associated with the response to anti-TNF therapy (Avila-Pedretti et al., 2015) and co-localized with NF-κB(p65) (Figure 1K). To get further insights into the potential association, we treated the RAW264.7 cells with TNF-α at different doses and time points (Figures 3D–3G and S6). We found that TNF-α upregulated the expression of RGS12, pNF-κB (phospho-NF-κB p65 (Ser536)), and pIκBα (phospho-IκBα (Ser32)) in both dose- and time-dependent manners (Figures 3D–3G). To further confirm whether RGS12 directly regulates the phosphorylation of NF-κB(p65) and IκBα, BMMs were isolated from *RGS12*$^{fl/fl}$ and the *LysmCre*$^{+}$;*RGS12*$^{fl/fl}$ and treated with TNF-α for 0, 15, 30, and 60 min. We found the deletion of RGS12 inhibited TNF-α stimulated the phosphorylation of NF-κB(p65) and pIκB (Figures 3H–3J). Moreover, forced expression of RGS12 upregulated pNF-κB(p65) expression but had no effect on NF-κB(p65) mRNA and total protein levels (Figures S3A and S3B). These findings suggest that RGS12 plays an essential role in inflammation-stimulated activation of NF-κB(p65) and IκB.

RGS12 Associates with NF-κB(p65) to Promote NF-κB(p65) Phosphorylation and Nuclear Translocation

To further identify the relationship between RGS12 and NF-κB(p65), we performed co-immunoprecipitation (Co-IP) and found that RGS12 associated with NF-κB(p65) in RAW 264.7 cells (Figure 4A). RGS12 contains six functional domains (PDZ, PTB, RGS, RBD1, RBD2, and GoLoco) (Figure 4B). To further determine which RGS12 domain affects the association with NF-κB (p65), we created six RGS12 mutations by deleting the specific functional domain as shown in Figure 4B. We found that the deletion of the RGS12 PTB domain impaired the association between RGS12 and NF-κB(p65) (Figure 4C), demonstrating that PTB domain promotes the association of RGS12 and NF-κB(p65). Moreover, to explore whether RGS12 regulates NF-κB(p65) nuclear translocation during inflammation, RAW264.7 cells were treated with LPS at different

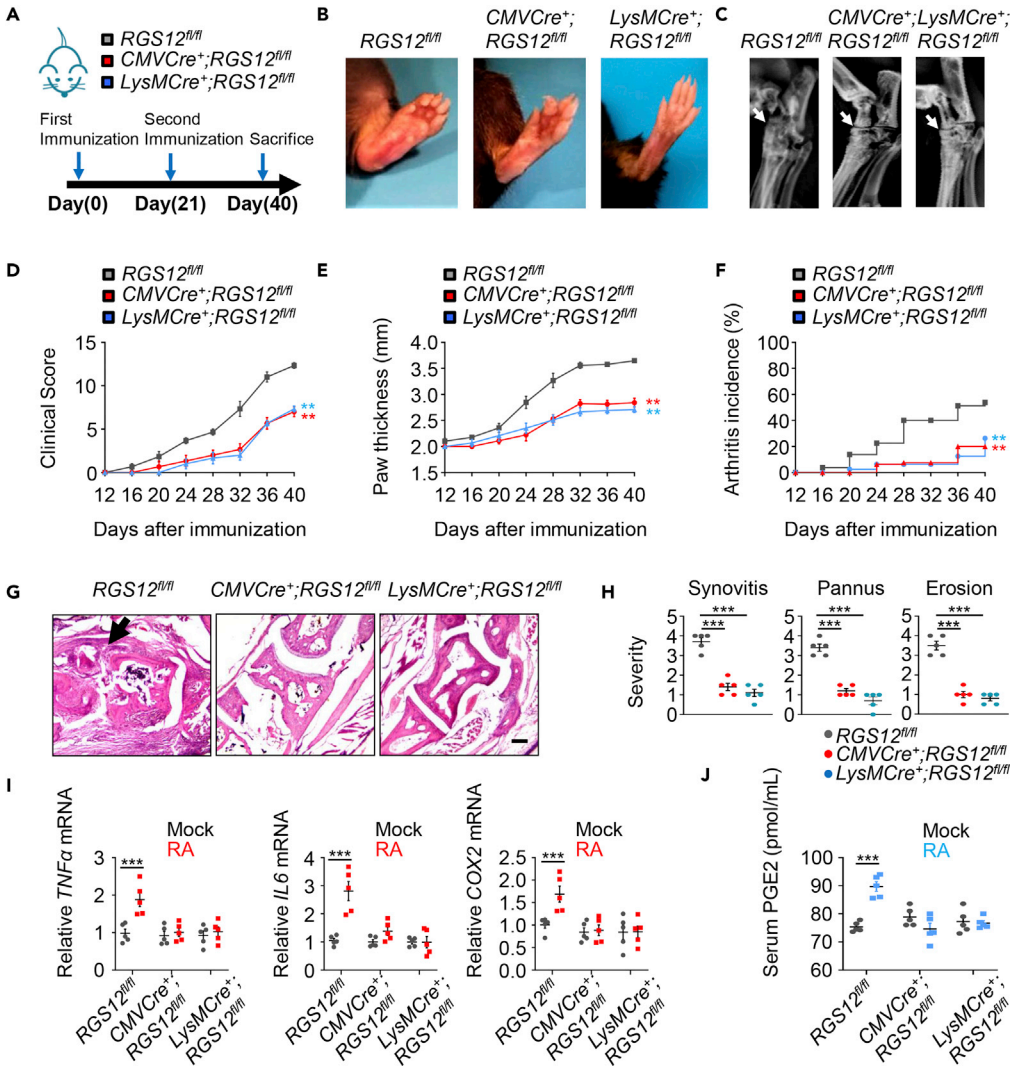

Figure 2. Deletion of RGS12 in Macrophages Inhibits the Spontaneous Development of Inflammatory Arthritis in CIA Mice

(A) Graphical representation of the experimental strategy. CIA was induced in *RGS12*$^{fl/fl}$ (gray), *CMVCre*$^{+}$; *RGS12*$^{fl/fl}$ (blue), and *LysMCre*$^{+}$; *RGS12*$^{fl/fl}$ (red) mice derived from C57BL/6 strain by subcutaneous injection of chicken type II collagen in enriched CFA (First immunization, day 0) and subsequent challenge with type II collagen in incomplete Freund's adjuvant (IFA) (Second immunization) on day 21. After the immunization for 40 days, RA mice were sacrificed (see also Figure S2).

(B) Paws of *RGS12*$^{fl/fl}$, *CMVCre*$^{+}$; *RGS12*$^{fl/fl}$ and *LysMCre*$^{+}$; *RGS12*$^{fl/fl}$ mice derived from C57BL/6 strain (n = 5 mice/group) were immunized with chicken type II collagen for 40 days.

(C) Radiography of ankle joints of *RGS12*$^{fl/fl}$, *CMVCre*$^{+}$; *RGS12*$^{fl/fl}$ and *LysMCre*$^{+}$; *RGS12*$^{fl/fl}$ CIA mice. White arrow shows severe joint destruction in *RGS12*$^{fl/fl}$ CIA mice compared with the RGS12-deficient mice.

(D) Clinical arthritis scores in *RGS12*$^{fl/fl}$, *CMVCre*$^{+}$; *RGS12*$^{fl/fl}$ and *LysMCre*$^{+}$; *RGS12*$^{fl/fl}$ mice with CIA. Data are presented as the mean ± SEM. **p < 0.01 versus the control *RGS12*$^{fl/fl}$ group (n = 5).

(E) Changes of paw thickness in the indicated groups.

(F) Incidence of arthritis in the indicated groups.

(G) Hematoxylin and eosin (H&E) staining for RA synovial tissue samples.

(H) Quantitative evaluation of synovitis, pannus formation, and erosion of tarsal joints in (G). Scale bar, 200 mm. Values are mean ± SEM. ***p < 0.001 versus the control *RGS12*$^{fl/fl}$ group, (n = 5).

(I) Real-time PCR analysis for the expression of *TNFα*, *IL6*, and *COX2* in synovium tissue relative to *RGS12*$^{fl/fl}$ group (n = 5).

(J) ELISA test for serum PGE2 levels in *RGS12*$^{fl/fl}$, *CMVCre*$^{+}$; *RGS12*$^{fl/fl}$ and *LysMCre*$^{+}$; *RGS12*$^{fl/fl}$ mice with CIA. Data are presented as the mean ± SEM. ***p < 0.001 versus the control *RGS12*$^{fl/fl}$ group (n = 5).

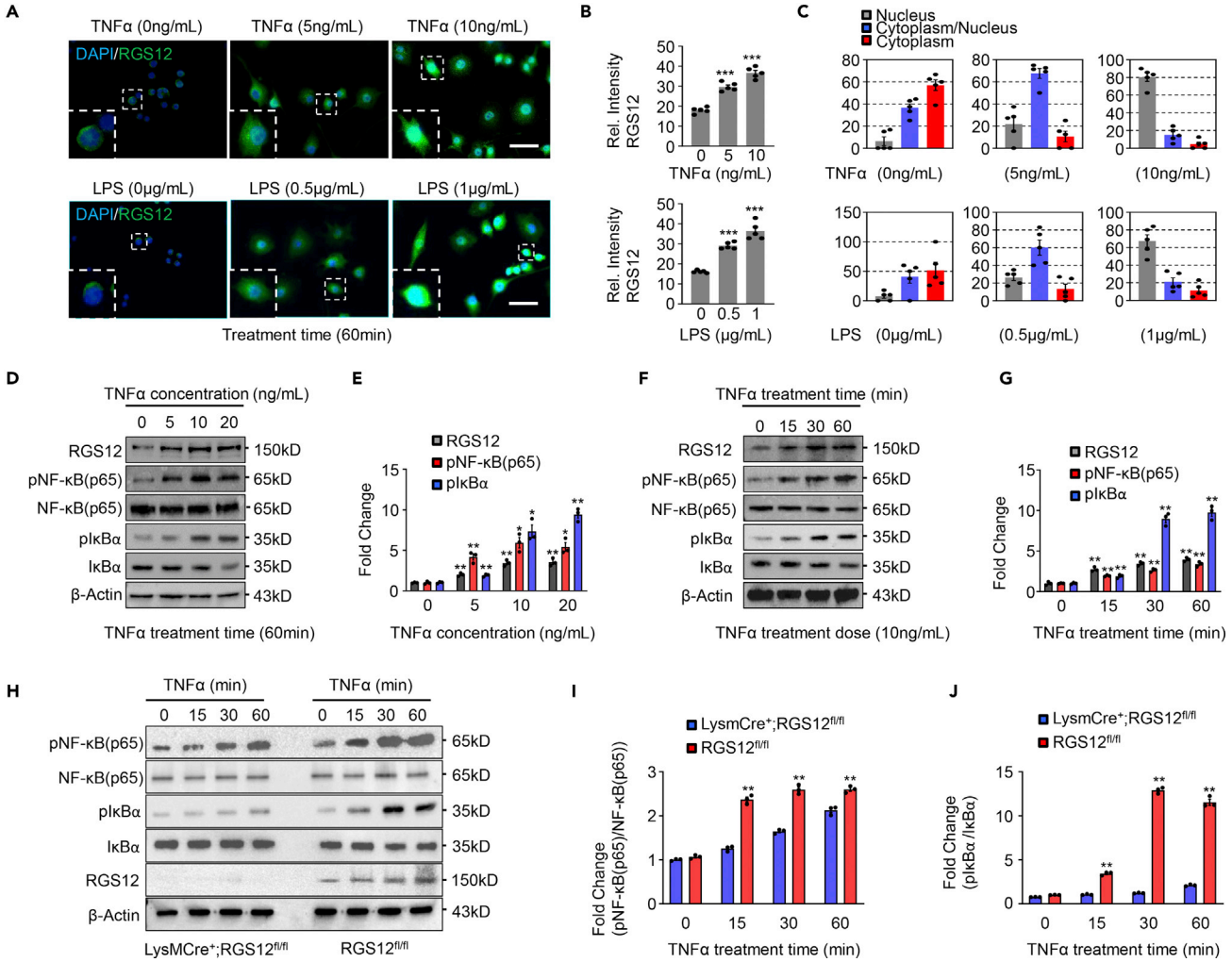

Figure 3. RGS12 Is Essential for the Phosphorylation of NF-κB(p65) and IκBα

(A) Left: Immunofluorescence staining for RGS12 expression in BMMs treated with different doses of TNF-α (0, 5, and 10 ng/mL) and LPS (0, 0.5, and 1 μg/mL). Scale bar, 50 μm. Representative individual and overlaid images are shown.

(B) Quantification of RGS12 expression in (A), measured by the ImageJ densitometry method. Data are presented as the mean ± SEM. ***$p < 0.001$ versus the control group, n = 5.

(C) TNF-α and LPS induce nuclear translocation of RGS12 in BMMs as depicted in (A). Quantitative data showed the subcellular location of RGS12. Gray, nucleus; blue, cytoplasm and nucleus; red, cytoplasm.

(D) Protein expression levels of RGS12, pNF-κB (Phospho-NF-κB p65 (Ser536)), NF-κB(p65), pIκBα (Phospho-IκBα (Ser32)), IκBα, and β-Actin following treatment of TNF-α with different doses (0, 5, 10, and 20 ng/mL) in RAW264.7 cells for 60 min.

(E) Blots underwent semi-quantitative analysis of RGS12, pNF-κB(p65), and pIκBα in (D) (n = 3). Data are the mean ± SEM. **$p < 0.01$ versus TNF-α untreated group.

(F) Protein expression levels of RGS12, pNF-κB(p65), NF-κB(p65), pIκBα, IκBα, and β-Actin following treatment of TNF-α with 10 ng/mL in RAW264.7 cells for 0, 15, 30, and 60 min.

(G) Quantitative analysis of RGS12, pNF-κB(p65), and pIκBα in (F) (n = 3). Data are mean ± SEM. **$p < 0.01$ versus TNF-α untreated group.

(H) RGS12 deficiency in macrophages inhibits pNF-κB(p65) and pIκBα expression in TNF-α-mediated inflammation *in vitro*. The BMMs were isolated from *LysMCre^{+}; RGS12$^{fl/fl}$* and *RGS12$^{fl/fl}$* mice and then incubated with TNF-α (10 ng/mL) for 0, 15, 30, and 60 min (see also Figure S6).

(I) The expression of pNF-κB(p65) in (H) was analyzed by western blots. NF-κB(p65) as an internal control. Note that the loss of RGS12 decreases the pNF-κB(p65) after TNF-α treatment. Data are mean ± SEM. **$p < 0.01$ versus *RGS12$^{fl/fl}$* group. The representative of three experiments.

(J) The expression of pIκBα in (H) was analyzed by western blots. IκBα as an internal control. Note that the loss of RGS12 decreases the pIκBα expression after TNF-α treatment. Data are mean ± SEM. **$p < 0.01$ versus *RGS12$^{fl/fl}$* group, (n = 3).

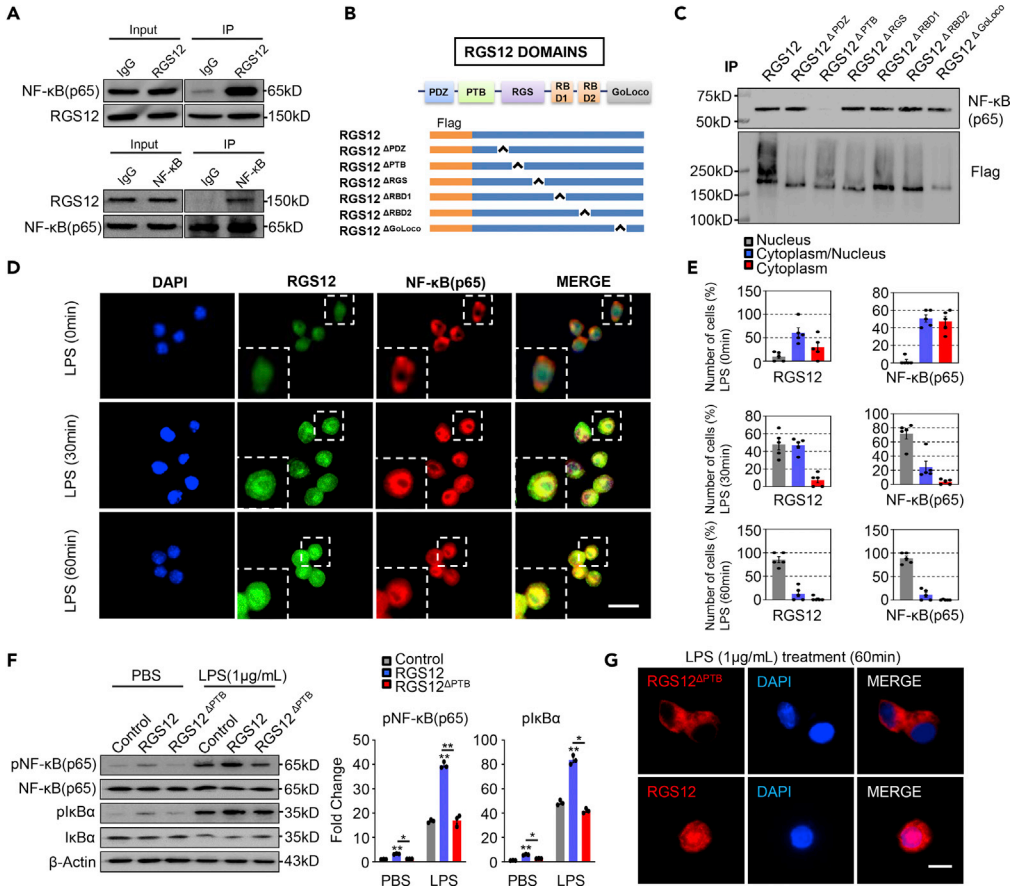

Figure 4. RGS12 Associates with NF-κB(p65) to Promote NF-κB(p65) Phosphorylation and Nuclear Translocation

(A) RGS12 interacts with NF-κB(p65) in RAW264.7 cells (Co-IP assay). The cell lysates were incubated with anti-RGS12 or control immunoglobulin G (IgG) antibodies, and the bound protein was examined by western blotting (WB) with the corresponding antibodies.

(B) Schematic diagram of RGS12 domain mutations. Functional domains are shown in the top. *FLAG-tagged RGS12* and *FLAG-tagged RGS12 domain mutations* (lack of one functional domain) are constructed into the *p3xFLAG-Myc-CMV-26* vector.

(C) RGS12 PTB domain is required for the interaction with NF-κB(p65). RAW264.7 cells were co-transfected with a series of expression vectors as described in the method section. NF-κB(p65) protein was immunoprecipitated by FLAG antibody, and abundance of coimmunoprecipitated proteins was determined by western blotting using anti-NF-κB(p65) or anti-FLAG antibodies.

(D) Co-localization of RGS12 (green) and NF-κB(p65) (red) in RAW264.7 cells treated with LPS (1 μg/mL) across different time points (0, 30, and 60 min). The merged images showed co-localization (yellow to orange). Scale bar, 20 μm. Representative individual and overlaid images are shown.

(E) Quantitation of the subcellular distribution of RGS12 (left) and NF-κB(p65) (right). The subcellular localization was categorized as nuclear (gray), cytoplasmic and nuclear (blue), and cytoplasmic (red).

(F) Left panel: the expressions of pNF-κB(p65) and pIκBα in RAW264.7 cells with and without *RGS12* or *RGS12*$^{\Delta PTB}$ overexpression (OE) or LPS treatment. Western blotting was performed to analyze the expression of pNF-κB(p65) and pIκBα in RAW264.7 cells. RAW264.7 cells were transfected with vector plasmid DNA (*p3xFLAG-Myc-CMV-26*) (3 μg) and *RGS12* (3 μg) or *RGS12*$^{\Delta PTB}$ plasmid (3 μg) for 48 h, respectively, and cells of LPS groups were treated with LPS (1 μg/mL) for 1 h before harvest. Right panel: Densitometric evaluation of pNF-κB(p65) and pIκBα in RAW264.7 cells transfected with *RGS12* or *RGS12*$^{\Delta PTB}$ and exposed to LPS (n = 3). *p < 0.05, **p < 0.01, Values are means ± SEM. Data are representative of three separate experiments. Note that RGS12 without the PTB domain cannot increase the pNF-κB(p65) and pIκBα expression (see also Figure S4).

(G) The lack of a functional PTB domain in RGS12 inhibits nuclear translocation of RGS12. The cells were transiently transfected with construct encoding either *RGS12*$^{\Delta PTB}$ (top panels) or *FLAG-tagged RGS12* (bottom panels) for 48 h and treated with LPS (1μg/mL) for 60 min. Scale bar, 10 μm.

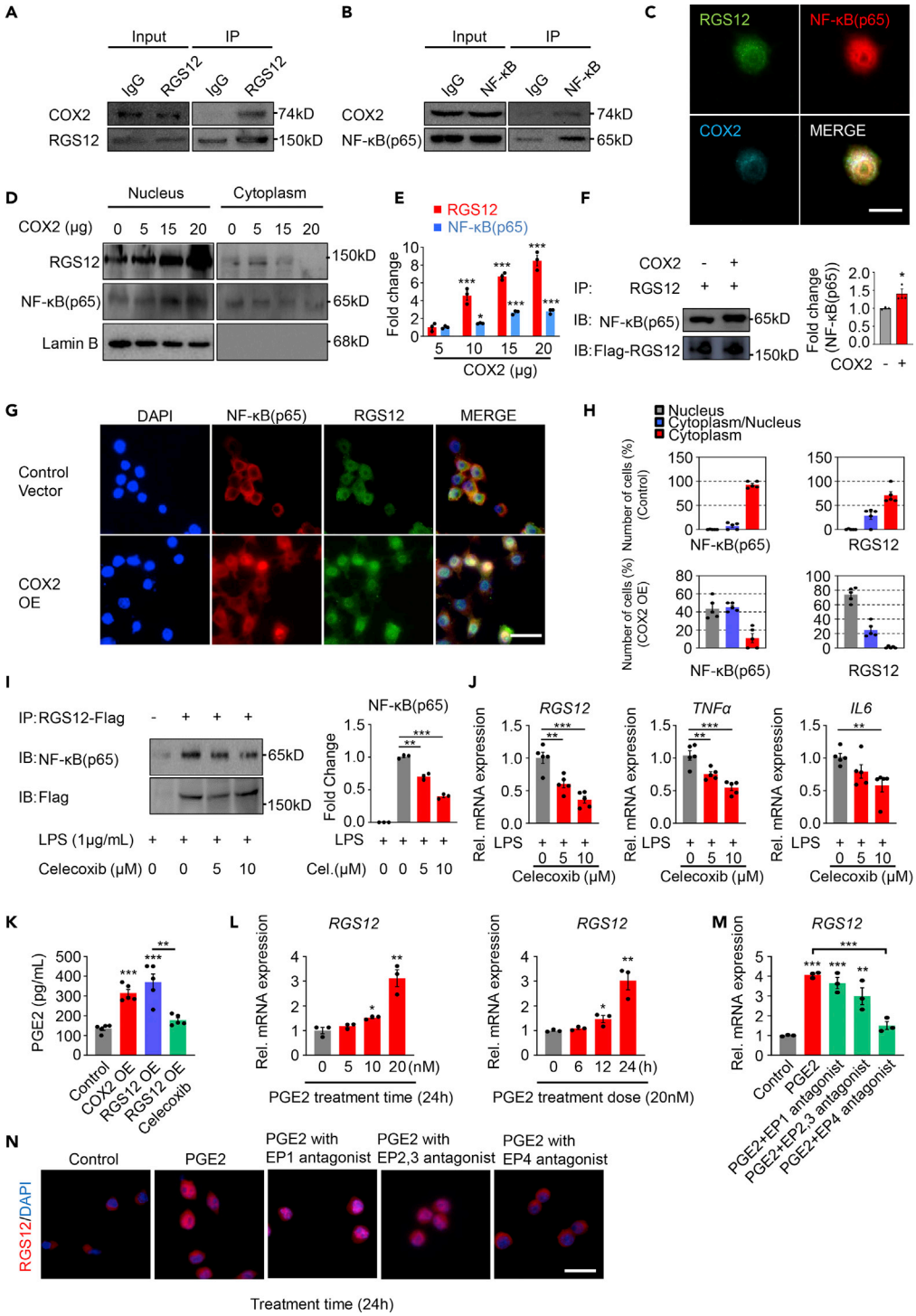

Figure 5. COX2 Promotes NF-κB(p65) and RGS12 Nuclear Translocation in Macrophages

(A and B) COX2 interacts with RGS12 and NF-κB(p65) in macrophages. The RAW264.7 cells were co-transfected with *COX2/RGS12* (A) or *COX2/NF-κB(p65)* (B), respectively. Cell lysates of macrophages were incubated with anti-RGS12, anti-NF-κB(p65), or control immunoglobulin G (IgG) antibodies, and bound protein was examined by western blotting (WB) with the corresponding antibodies.

(C) Co-localization of RGS12 (green), NF-κB(p65) (red), and COX2 (blue) in RAW264.7 cells treated with LPS (1 μg/mL) for 30 min. The merged images showed the co-localization (yellow to orange). Scale bar, 10 μm.

Figure 5. *Continued*

(D) Western blot analysis of nuclear translocation of RGS12 and NF-κB(p65) after RAW264.7 cells transfected with *COX2*at the indicated concentrations (0, 5, 15, and 20 μg) for 24 h.

(E) Densitometric evaluation of RGS12 and NF-κB(p65) for nuclear translocation in RAW264.7 cells as shown in (D). *$p < 0.05$, **$p < 0.01$ versus COX2 untreated group. Data are representative of three separate experiments. Note that nuclear translocation of RGS12 and NF-κB(p65) are enhanced by COX2 overexpression.

(F) RAW264.7 cells were transfected with/without *pCMV-COX2* (3 μg) and *pcDNA3.1-RGS12-FLAG* (3 μg). The cell extracts and the immunoprecipitates were analyzed by western blot. *$p < 0.05$, values are means ± SEM (n = 3).

(G) COX2-dependent nucleocytoplasmic shuttling of NF-κB(p65) and RGS12. RAW264.7 cells transiently transfected with control vector (*pCMV*) or *pCMV-COX2* (3 μg) for 24 h. The cells were then fixed and incubated with the anti-NF-κB(p65) or anti-RGS12 antibody followed by incubation with fluorescein isothiocyanate-conjugated secondary antibody. Note that the transfection of *COX2* constructs enhanced RGS12 and NF-κB(p65) nuclear translocation. Scale bar, 20 μm.

(H) Quantitative data on the subcellular localization of NF-κB(p65) (left) and RGS12 (right). Gray, nucleus; blue, cytoplasm/nucleus; red, cytoplasm.

(I) Ectopic RGS12 pulls down endogenous NF-κB(p65). RAW264.7 cells were transfected with RGS12-FLAG plasmid (10 μg) for 24 h and treated with LPS (1 μg/mL) and celecoxib (COX2 inhibitor) at the indicated concentrations (0, 5, and 10 μM) for 24 h. Cell lysates were immunoprecipitated with anti-FLAG antibody and analyzed for NF-κB(p65) by western blot. ***$p < 0.001$ and **$p < 0.01$, values are means ± SEM (n = 3).

(J) The mRNA expression of *RGS12, TNFα*, and *IL6* after treating with indicated concentration of celecoxib (0, 5, and 10 μM). *$p < 0.05$, **$p < 0.01$, ***$p < 0.001$, mean values are shown unless otherwise specified, and error bars represent ±SEM (n = 5).

(K) The RAW264.7 cells were forced overexpression of *COX2*, *RGS12* and treated with/without celecoxib (10 μM) for 24 h for detecting PGE2 level. **$p < 0.01$, ***$p < 0.001$ versus the control group (n = 5).

(L) mRNA expression levels of *RGS12* following treatment of PGE2 with different doses (0, 5, 10, and 20 ng/mL) (left) and time (0, 6, 12, and 24 h) (right) were determined. Data are mean ± SEM. **$p < 0.01$ versus PGE2 untreated group (n = 3).

(M) mRNA expression levels of *RGS12* following treatment of PGE2 (20 ng/mL) for 24 h without/with different EP antagonists (EP1, 17-phenyl trinor Prostaglandin E2 [10 μM]; EP2 and EP3, AH 6809 [10 μM]; EP4, AH 23848 [10 μM]). Data are mean ± SEM. **$p < 0.01$ versus PGE2 untreated group (n = 3).

(N) Nuclear translocation of RGS12 following treatment of PGE2 (20 ng/mL) for 24 h without/with different EP antagonists as described in (J). Note that EP4 antagonist (10 μM) inhibits nuclear translocation of RGS12 induced by PGE2 (20 ng/mL).

time points (0, 30 and 60 min). Interestingly, we found that RGS12 co-localized with NF-κB(p65), and both proteins were translocated to the nucleus within 60 min following LPS stimulation (Figures 4D and 4E). To further characterize the function of the PTB domain, stable cells that express *RGS12* or $RGS12^{\Delta PTB}$ were treated with LPS. The loss of the PTB domain reduced phosphorylation (Figure 4F) and nuclear translocation of NF-κB(p65) (Figure 4G). Consistently, overexpression of the *RGS12 PTB domain* in RAW264.7 cell increased the level of pNF-κB(p65) (Figure S4) but not the total NF-κB(p65), suggesting that RGS12 regulates NF-κB activation through its PTB domain.

COX2 Promotes the Nuclear Translocation of NF-κB(p65) and RGS12 in Macrophages

Previous studies have reported that COX2 expression increases in human RA and COX2 regulates NF-κB activity (Rao et al., 2005; Tipton et al., 2007). We found that LPS increases both RGS12 and COX2 expression in a dose-dependent manner (Figure S5). To determine whether COX2 affects RGS12/NF-κB(p65) signaling in RAW264.7 cells, we performed IP and found both RGS12 and NF-κB(p65) associated with COX2 (Figures 5A and 5B). Upon LPS treatment, COX2 co-localized with RGS12 and NF-κB(p65) in the exterior of the nucleus (Figure 5C). To further explore the relationship between COX2 and RGS12/NF-κB(p65), we overexpressed *COX2* in macrophages and found that overexpression of *COX2* enhanced the nuclear translocation of RGS12 and NF-κB(p65) in a dose-dependent manner (Figures 5D and 5E). This result was further confirmed by immunofluorescence staining results (Figures 5G and 5H). Moreover, we found that COX2 promoted the association of RGS12 and NF-κB(p65) (Figure 5F). In contrast, treatment of RAW264.7 cells with the different concentrations (0, 5, and 10μM) of COX2 inhibitor celecoxib and LPS (1μg/mL) decreased the association of RGS12 and NF-κB(p65) (Figure 5I) and downregulated the expression of *RGS12, TNFα*, and *IL6* (Figure 5J). Furthermore, we found that RGS12 overexpression increased PGE2 level, which was inhibited by the COX2 inhibitor celecoxib (Figure 5K). To further explore whether PGE2 also regulates RGS12 expression, we treated RAW264.7 cells with PGE2 in different doses (0, 5, 10, and 20 nM) and at different times (0, 6, 12, and 24 h) (Figure 5L). We found that PGE2 significantly promotes the expression of RGS12 in a dose- and time-dependent manner (Figure 5L). Moreover, blocking one of the PGE2 receptors, EP4 significantly impaired the PGE2-mediated increase of the RGS12 expression as well as nuclear translocation (Figures 5M and 5N). Blocking EP2 and EP3

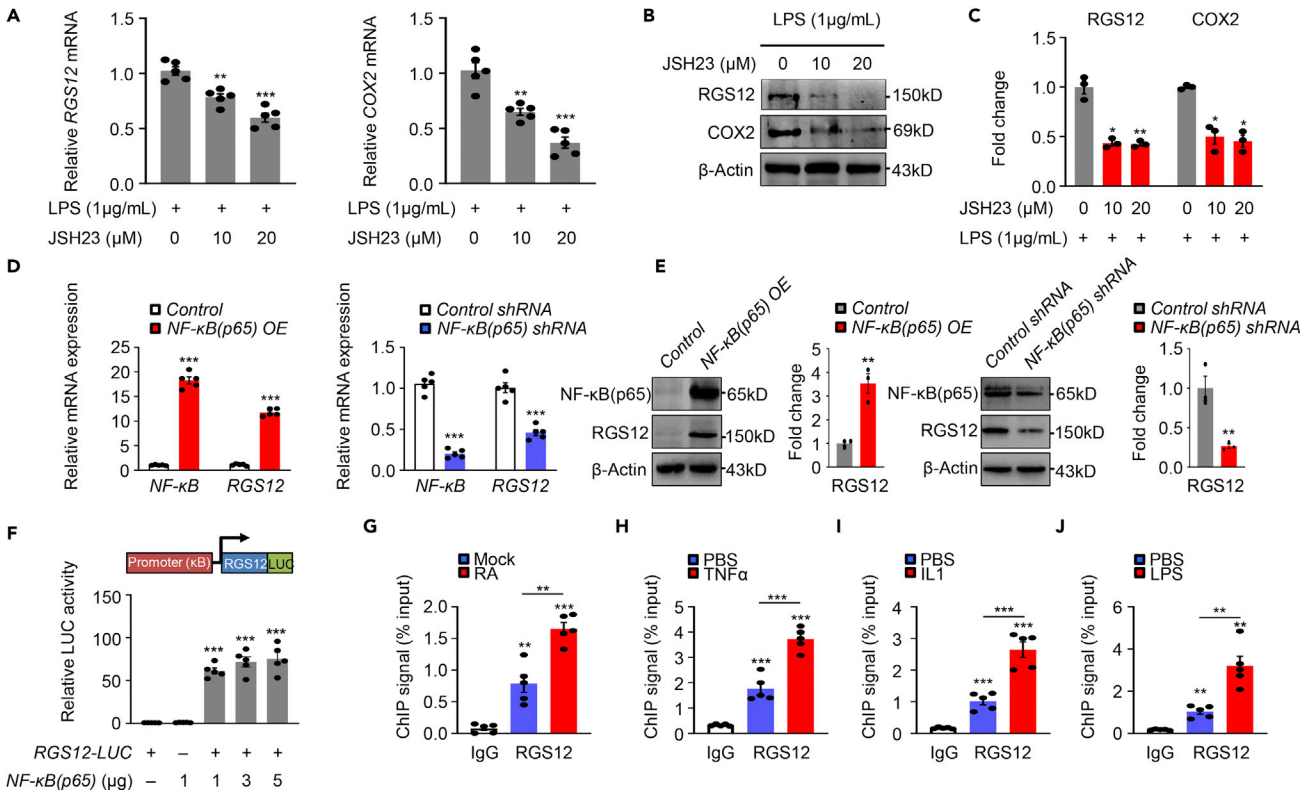

Figure 6. NF-κB Transcriptionally Regulates RGS12 Expression in Macrophages

(A) *RGS12* and *COX2* mRNA levels in RAW264.7 cells treated with LPS (1 μg/mL) and JSH23 (NF-κB inhibitor) at indicated concentrations (0, 10, and 20 μM) for 24 h **p < 0.01, ***p < 0.001 versus the control group (n = 5).

(B) Western blot analysis of RGS12 and COX2 expression profile in RAW264.7 cells treated by LPS (1 μg/mL) and JSH23 at indicated concentration (0, 10, and 20 μM) for 24h.

(C) Quantitation of RGS12 and COX2 protein levels as shown in (B). The data are normalized to β-Actin. *p < 0.05, **p < 0.01 versus the control group (n = 3).

(D) The relative gene expression levels showing that overexpression of *NF*-κB(p65) (*NF-κB(p65) OE*) increased *NF-κB(p65)* and *RGS12* levels, *NF-κB(p65) shRNA* decreased the expression of *NF-κB(p65)* and *RGS12*. The t test showed significant differences between the two groups, ***p < 0.001 versus control (n = 5).

(E) Immunoblot showed the NF-κB(p65) and RGS12 protein level in NF-κB(p65) overexpression (*NF-κB(p65) OE*) or NF-κB(p65) knockdown (*NF-κB(p65) shRNA*) condition. Quantitative data showed the relative levels of RGS12 (quantified with NIH ImageJ software). A t test showed significant differences between the two groups, *p < 0.05, **p < 0.01 versus Control. Data are representative of three separate experiments.

(F) 293T cells were co-transfected with the *RGS12-LUC reporter* (1 μg) and combinations of plasmids expressing *NF-κB(p65)* (1, 3, and 5 μg) for 24 h. The overexpression of *NF-κB(p65)* results in higher RGS12 activation (p < 0.001).

(G) ChIP assays from Mock and RA SMs showing RGS12 and IgG control at κB site. ChIP was analyzed by quantitative PCR. A t test showed significant differences between the two groups, **p < 0.01, ***p < 0.001 versus Control (n = 5).

(H–J) ChIP assays from RAW264.7 cells showing NF-κB(p65) at RGS12 κB site after introduction of control PBS or TNF-α (10 ng/mL) (H), IL-1(10 ng/mL) (I), and LPS (1 μg/mL) (J). **p < 0.01, ***p < 0.001 versus the control group (n = 5).

antagonists minorly inhibited the RGS12 level and nuclear translocation, whereas EP1 antagonist did not affect the RGS12 expression (Figures 5M and 5N). Thus, our results demonstrated that COX2 may regulate RGS12 mainly through the PGE2-EP4 pathway.

NF-κB(p65) Transcriptionally Regulates RGS12 Expression in Macrophages

We first tested whether the inhibition of NF-κB affects RGS12 expression level in the LPS-treated RAW264.7 cells. As expected, inhibition of NF-κB(p65) using inhibitor JSH23 reduced the expression levels of RGS12 and COX2 (Figures 6A–6C). To investigate the transcriptional regulation role of NF-κB(p65), we overexpressed or silenced NF-κB(p65) in RAW264.7 cells. The results showed that overexpression of NF-κB(p65) increased RGS12 expression; in contrast, the silence of NF-κB(p65) decreased the expression of RGS12 (Figures 6D and 6E). To further test whether RGS12 acts as a transcriptional target of NF-κB(p65),

293T cells were co-transfected with the *RGS12-luciferase* reporter vector and different concentrations of *NF-κB(p65)* vectors. The results showed that NF-κB(p65) promoted RGS12 expression in 293T cells in a dose-dependent manner (Figure 6F). We then analyzed the sequences of *RGS12* and found the κB-binding motifs (GGGGCTTCC) locate in the *RGS12* promoter region. To determine whether NF-κB(p65) binds to the κB motif of the RGS12 promoter region, chromatin immunoprecipitation (ChIP) assay was performed in SMs isolated from wild-type (WT) mice without or with RA. We found that NF-κB(p65) directly bound to this κB motif (GGGGCTTCC) and that the binding level was increased in RA mice compared with the control (Figure 6G). This enhanced binding was also found in the TNF-α (Figure 6H), IL1 (Figure 6I), and LPS (Figure 6J)-induced RAW264.7 cells.

Treatment with Nanoparticles Containing *RGS12 shRNA* Blocks the Progression of Chronic Arthritis in Mice

To determine whether inhibition of RGS12 can block the inflammatory response in macrophages, we constructed *RGS12 shRNA* silence vectors (*psi-nU6.1-shRGS12*), transfected *shRGS12* into RAW264.7 cells, and then treated them with LPS. The silence of RGS12 inhibited transcript and protein expression of enzymes or inflammatory factors such as COX2, TNF-α, and IL-6 *in vitro* (Figures 7A and 7B). To determine whether *shRGS12* can inhibit inflammatory responses through the suppression of NF-κB(p65) nuclear translocation, we transfected the *shRGS12* plasmid into BMMs with or without LPS treatment. The result showed that the silence of RGS12 impaired NF-κB(p65) nuclear translocation during the inflammatory state (Figure 7C). We next sought to examine the therapeutic efficacy of *shRGS12* on inhibiting RA progression. By delivering *shRGS12*-nanoparticles to mice with established mild arthritis (clinical score 8–10) every 3 days for 14 days (Figure 7D), we found that *shRGS12*-nanoparticles reduced RGS12 protein levels in control and RA groups (Figure 7E). Treatment of RA mice with *shRGS12*-nanoparticles for 14 days resulted in the elimination of visual signs of arthritis (Figure 7F), a significant reduction of arthritis severity score and paw swelling, (Figure 7G) and reduced inflammatory cell infiltration in the synovium (Figure 7H). Taken together, these data demonstrated that inhibition or silence of RGS12 is a promising strategy for the treatment of inflammatory arthritis.

DISCUSSION

For the first time, we found a critical role of RGS12 in regulating inflammation through activating a RGS12-NF-κB feedback loop (Figure 8). The major findings of this study are: first, LPS, TNF-α, and PGE2 associate with their receptors such as TNFR/TLR and EP receptors to trigger the RGS12 expression; second, the increased RGS12 promotes the phosphorylation of NF-κB and IκB, IκB proteolysis, and nuclear translocation of NF-κB; third, deletion or silence of RGS12 in macrophages inhibits the release of pro-inflammatory cytokines in RA, through the reduced activation of NF-κB(p65); fourth, PTB domain promotes the association of RGS12 and NF-κB(p65), and NF-κB(p65) inversely regulates the transcription of the RGS12 gene, which forms an auto-regulatory feedback loop; last but not least, COX2 enhances nuclear translocation of RGS12/NF-κB(p65) in inflammatory conditions. Thus, RGS12 is a critical NF-κB activator in the pathogenesis of inflammatory arthritis.

Macrophages are one of the most abundant cell types in the RA synovium and are critical drivers in the progression of RA (Sack et al., 1994). Interestingly, after analyzing the GEO data (Database: GSE49604) from control subjects and patients with RA (You et al., 2014), we found that the expression of the longest isoform of *RGS12* (isoform 2, GenBank: NM_002926.3), which contains PDZ-PTB domains and specialized C terminus, showed a more significant change in RA macrophages (Figure 2). Similarly, our real-time PCR data showed the long RGS12 isoforms (isoform 1 and 2) with the PTB domain significantly increased in RA synovium. The longest isoform 2 was increased the most in RA, which may be due to the specialized C terminus enhancing its function. However, RGS12 isoform 3 (short isoform) without the PTB domain did not show any significant change (Figure 1C), suggesting that isoform 3 may not be able to regulate inflammation in RA. Additionally, these findings were consistent with our results showing that the RGS12 longest isoform was highly expressed in synovial RA macrophages in human RA samples and CIA mouse models (Figures 1C, 1D, and 1J–1L).

Our results showed that global deletion of RGS12 alleviated the RA phenotype in mice (Figure 2), which was replicated in the RGS12 conditional knockout model targeted to monocytes/macrophages, indicating that RGS12 plays an important role in macrophages of RA. However, besides macrophages, T cells, B cells, and the orchestrated interaction of pro-inflammatory cytokines also play important roles in the

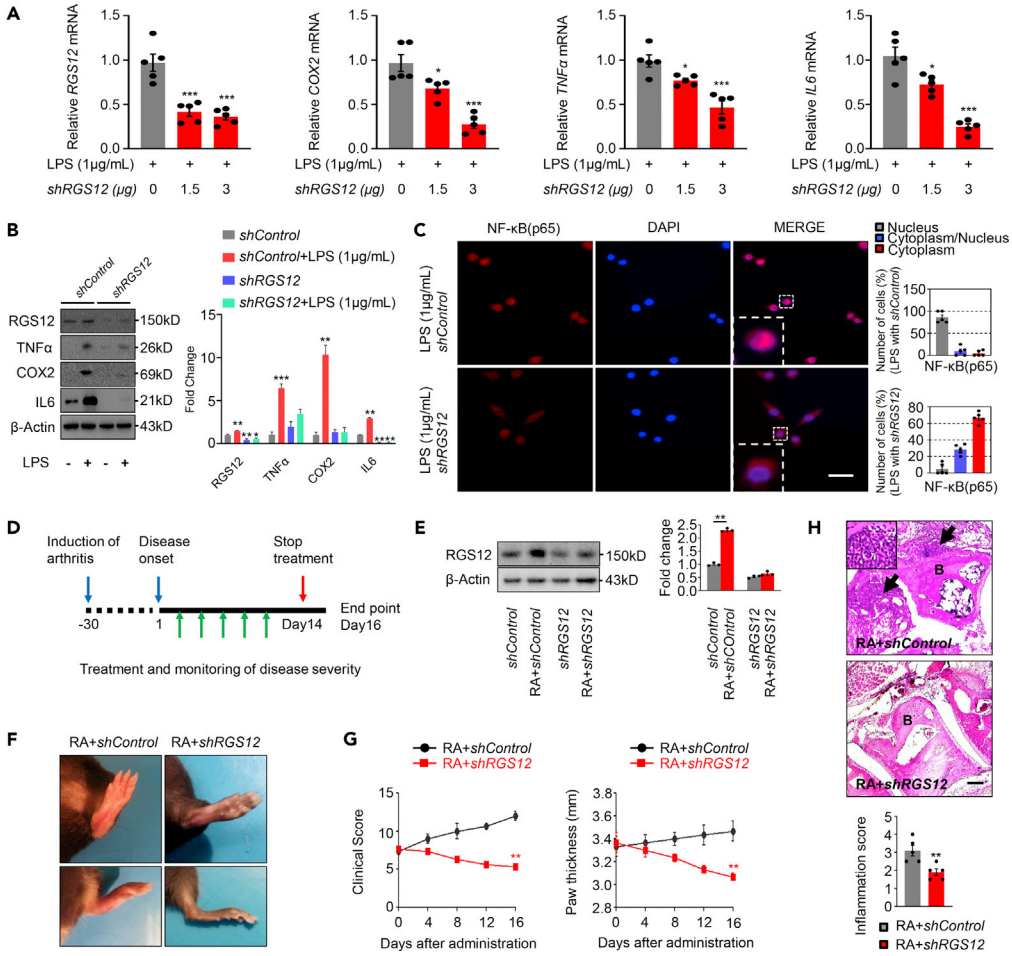

Figure 7. Treatment with Nanoparticles Containing *RGS12 shRNA* Blocks the Progression of Chronic Arthritis in Mice

(A) The mRNA expression of *RGS12*, *COX2*, *IL6*, and *TNFα* in RAW264.7 cells after treating with LPS (1 μg/mL) and shRGS12 at indicated concentrations (0, 1.5, and 3 μg) were evaluated by qPCR. Data were analyzed by unpaired t test, and asterisks on the graphs indicate p values of significance, *p < 0.05, ***p < 0.001.

(B) Left: western blot analysis for RGS12, TNF-α, COX2, and IL-6 expression in BMMs transfected with shRGS12 (3 μg) for 24 h and treated with or without LPS (1 μg/mL) for 24 h. Right: densitometric evaluation of RGS12, TNF-α, COX2, and IL-6. *p < 0.05, **p < 0.01, ***p < 0.001 versus shControl group. Data are representative of three separate experiments.

(C) Left panel: BMMs were transfected without or with *shRGS12* (3 μg) for 48 h and treated with LPS (1 μg/mL) for 24 h. Note that the transfection of *shRGS12* inhibits NF-κB(p65) nuclear translocation. Right panel: quantitative data on the subcellular localization of NF-κB(p65). Scale bar, 50 μm. Representative individual and overlaid images are shown.

(D) Graphical representation of the experimental strategy. CIA was induced in wild-type mice (C57BL/6) by subcutaneous injection of chicken type II collagen in enriched CFA and subsequent challenge with chicken type II collagen in incomplete Freund's adjuvant (IFA) on day 21. After the first immunization for 30 days, the mild RA mice (clinical score 8–10) received 10 μg of *shRGS12* nanoparticles or *shControl* nanoparticles into both the ankle joint cavities every 3 days during a 14-day course of therapy.

(E) Left: western blot analysis of RGS12 expression in synovial tissue from RA + *shControl* and RA + *shRGS12* treatment mice. Right: quantitation of RGS12 protein levels. The data are normalized to β-Actin. **p < 0.01 versus the control group (n = 3).

(F) Photographs showing the paw swelling in RA + *shControl* and RA + *shRGS12* nanoparticles-treated mice (n = 5/group).

(G) Clinical arthritis scores and paw thickness in the indicated groups. Data are presented as the mean ± SEM. *p < 0.05, **p < 0.01 versus the control.

(H) H&E staining shows a decrease in the local recruitment of inflammatory cells within synovial tissue (black arrows) in the *shRGS12* treatment group (B, bone area). **p < 0.01, n = 5. Scale bar, 200 μm.

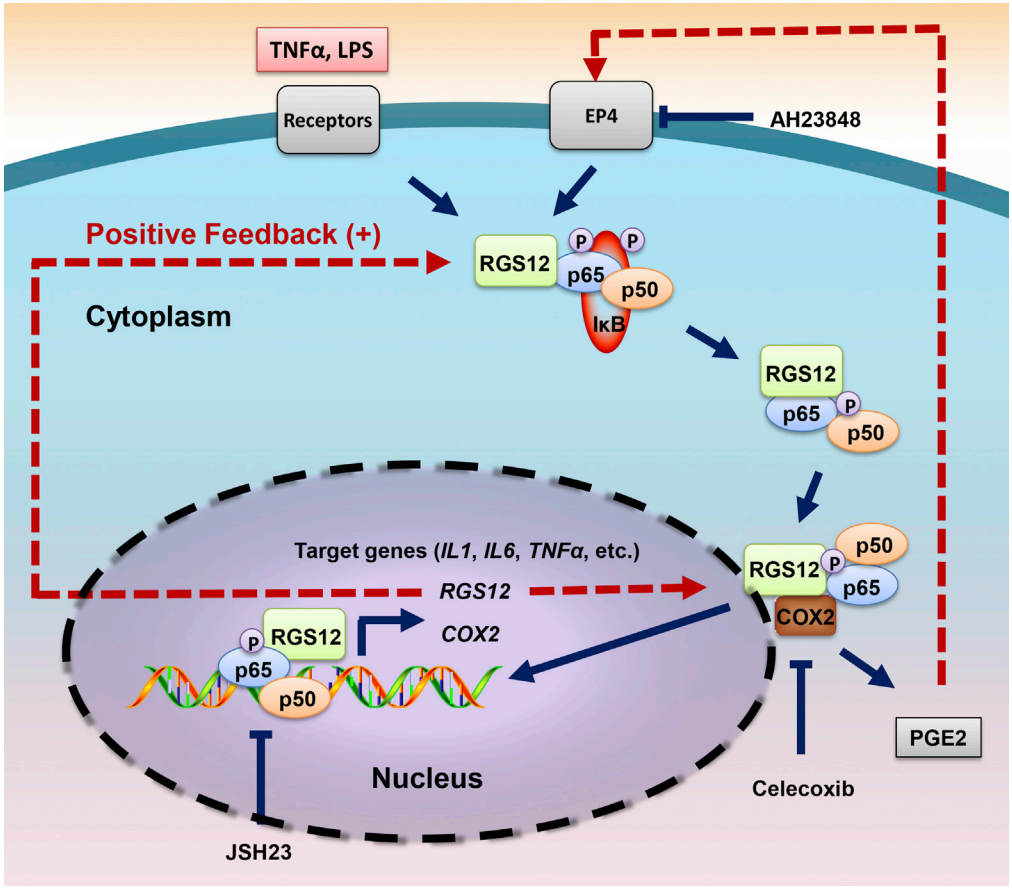

Figure 8. Proposed Model of RGS12 Regulation of Inflammation via Activating a RGS12-NF-κB Positive Feedback Loop

First, TNF-α and LPS or PGE2 associate with their receptors to promote the RGS12 expression. RGS12 associates with NF-κB(p65) to activate its phosphorylation and nuclear translocation of both proteins, which can be enhanced by association with COX2 on the nuclear membrane. Inhibition of COX2 by celecoxib reduces the RGS12/NF-κB(p65) complex association and inhibits their activation. Then, nuclear NF-κB(p65) increases the expression of inflammatory cytokines such as *IL1*, *IL6*, and *TNFα*, as well as enhances the expression of *RGS12* and *COX2* through transcriptional activation. Meanwhile, enhanced RGS12 further activates the phosphorylation and nuclear translocation of NF-κB(p65) in the cytoplasm, which forms a positive feedback loop. In addition, enhanced COX2 further increases the RGS12/NF-κB(p65) nuclear translocation and increases PGE2 production. PGE2 then promotes RGS12 activation through binding the membrane receptor EP4.

pathophysiology of RA (Matsumoto et al., 1999). Whether RGS12 plays a role in T/B cells or other cells needs to be further studied. Although the DBA/1 strain was found to be more susceptible to collagen type II arthritis and developed more severe arthritis than the C57BL/6 strain, the C57BL/6 strain was also suitable for RA research (Inglis et al., 2007). Our results showed that chicken type II collagen method was able to induce arthritis in C57BL/6 mice with an average incidence of 53.8% on day 40 after primary immunization, which was able to replicate the typical pathological process of RA. Those results were supported by other reports showing that chicken type II collagen could induce arthritis in C57BL/6 mice (Asquith et al., 2011; Chrobak et al., 2015; Park et al., 2015), with a maximum incidence of 61.7% and mean day of onset of 29.4 ± 1.3 days after primary immunization (Inglis et al., 2007).

RA is a complex immune system disease that is regulated by multiple factors. We observed that RGS12 expression in SMs increased during joint inflammation (Figure 2), which contributes to the enhanced nuclear translocation and activity of NF-κB (Figure 3). It has been proven that RGS12 directly interacts with the tyrosine-phosphorylated calcium channel through its PTB domain in neuronal cells (Schiff et al., 2000). Interestingly, the PTB domain of RGS12 is unique, which does not contain any of the conserved

Arg or Lys residues required by Shc (Src homology 2 domain containing) or IRS (Insulin receptor substrate) for phosphotyrosine coordination (Uhlik et al., 2005). Most recently, Schroer et al. reported that the RGS12 PTB domain binds to the specific phosphoinositides and then is localized to early endosomes in cultured myoblasts (Schroer et al., 2019; Willard et al., 2007). Here, we found that the PTB domain is essential for association of RGS12 and NF-κB(p65) to further promote the NF-κB(p65) activation. NF-κB contains different phosphorylation sites, which can be affected by various kinases. For example, c-Src and Lck are involved in the tyrosine phosphorylations of IκB-α and p65 NF-κB under silica induction (Kang et al., 2006). Phosphorylation of NF-κB is regulated by BDNF via its receptor tyrosine kinase TrkB (Gavalda et al., 2009). Thus, it is possible that the PTB domain of RGS12 can promote phosphorylation of NF-κB via enhancing the activity of a certain kinase. Meanwhile, the RGS12 PTB domain may promote NF-κB to expose more phosphorylation sites by binding and changing the spatial structure. Although the precise mechanism needs to be further defined, our results suggest that the PTB domain of RGS12 may be a potential therapeutic target for inflammation. Importantly, NF-κB activation and its downstream inflammatory response can be inhibited by the introduction of *shRGS12* both *in vivo* and *in vitro*, suggesting inhibition of RGS12 is a promising new therapeutic strategy for RA or other inflammatory diseases.

COX2 is a key intracellular enzyme in RA (Rao et al., 2005), which is monotopically inserted in the nuclear membrane to take up released arachidonic acid (Funk, 2001) and produce PGE2. Our results showed that COX2 acts as a chaperone to translocate the RGS12/NF-κB complex from the cytoplasm to the nucleus, suggesting COX2 plays an important role in RGS12/NF-κB signaling transduction. PGE2 acts in an autocrine and paracrine manner via a family of GPCR receptors termed EP1–EP4. However, whether RGS12 regulates Eps-mediated signaling regulation is unknown. Some studies have reported that EP1 regulates Ca^{2+} mobilization via Gαq and EP3 inhibits adenylyl cyclase via Gαi (Goulet et al., 2004). EP2 and EP4 regulate intracellular adenosine-3′,5′-cyclic monophosphate (cAMP) through Gαs. Moreover, EP4 associates with a pertussis toxin-sensitive inhibitory G-protein, Gαi (Fujino and Regan, 2006). In our study, we found that PGE2 can increase in RGS12 expression and NF-κB(p65) nuclear translocation and activation through EP4. Moreover, activated NF-κB(p65) further promotes the production of RGS12 and COX2/PGE2. Thus, these findings suggest that COX2-mediated PGE2/EP4 signaling and RGS12/NF-κB(p65) signaling may form a positive feedback regulation loop for inflammatory regulation (Figure 8).

In conclusion, our work provides strong evidence and critical mechanistic insights into a key role of RGS12 in inflammation. These findings will enable future studies to facilitate the design of clinical treatments for difficult-to-treat inflammatory diseases such as RA.

Limitations of the Study

Our studies were mainly performed on mouse models. Although mouse models are heavily used in preclinical studies, the onset time, intensity, and pathophysiological characteristics of rheumatoid arthritis are different from human clinical conditions. We refined our methods and mouse models to closely reflect human conditions; however, the differences in mouse anatomy and physiology may potentially limit the translational value of our conclusions. In addition, our study was limited only to the long isoforms of RGS12 on mouse models; therefore, further clinical trials are needed to validate our findings acquired from mouse models.

Resource Availability

Lead Contact

Further information and requests for resources and reagents should be directed to and will be fulfilled by the Lead Contact, Dr. Shuying Yang (shuyingy@upenn.edu).

Materials Availability

This study did not generate new unique reagents.

Data and Code Availability

The whole-genome microarray data were obtained using accession numbers GSE49604 at Gene Expression Omnibus (GEO).

METHODS

All methods can be found in the accompanying Transparent Methods supplemental file.

SUPPLEMENTAL INFORMATION

Supplemental Information can be found online at https://doi.org/10.1016/j.isci.2020.101172.

ACKNOWLEDGMENTS

This work was supported by grants from the National Institute on Aging (NIA) (R01AG048388) and National Institute of Arthritis and Musculoskeletal and Skin Diseases (NIAMS) (R01AR066101) to S.Y. We would like to acknowledge Micro-CT and histological Core facilities of the Penn Center for Musculoskeletal Disorders (PCMD), supported by NIH/NIAMS P30-AR069619. We also would like to thank Drs. Min Liu and Yan Yan for providing technical support and training for histology analysis.

AUTHOR CONTRIBUTIONS

S.Y and G.Y. planned the experiments and interpreted the results. G.Y. performed and analyzed most of the experiments with input from S.Y., A.N., S-T. Y., C.F.. L.X., M.J.O. provided advice on the mechanism studies. S.Y., G.Y., L.X., and M.J.O. conceived the project and wrote the manuscript with input from all authors.

DECLARATION OF INTERESTS

The authors declare no competing interests.

Received: August 8, 2019
Revised: December 15, 2019
Accepted: May 12, 2020
Published: June 26, 2020

REFERENCES

Alqinyah, M., Maganti, N., Ali, M.W., Yadav, R., Gao, M., Cacan, E., Weng, H.R., Greer, S.F., and Hooks, S.B. (2017). Regulator of G protein signaling 10 (Rgs10) expression is transcriptionally silenced in activated microglia by histone deacetylase activity. Mol. Pharmacol. *91*, 197–207.

Asquith, D.L., Miller, A.M., Reilly, J., Kerr, S., Welsh, P., Sattar, N., and McInnes, I.B. (2011). Simultaneous activation of the liver X receptors (LXRalpha and LXRbeta) drives murine collagen-induced arthritis disease pathology. Ann. Rheum. Dis. *70*, 2225–2228.

Avila-Pedretti, G., Tornero, J., Fernandez-Nebro, A., Blanco, F., Gonzalez-Alvaro, I., Canete, J.D., Maymo, J., Alperiz, M., Fernandez-Gutierrez, B., Olive, A., et al. (2015). Variation at FCGR2A and functionally related genes is associated with the response to anti-TNF therapy in rheumatoid arthritis. PLoS One *10*, e122088.

Bouta, E.M., Bell, R.D., Rahimi, H., Xing, L., Wood, R.W., Bingham, C.R., Ritchlin, C.T., and Schwarz, E.M. (2018). Targeting lymphatic function as a novel therapeutic intervention for rheumatoid arthritis. Nat. Rev. Rheumatol. *14*, 94–106.

Choi, S., You, S., Kim, D., Choi, S.Y., Kwon, H.M., Kim, H.S., Hwang, D., Park, Y.J., Cho, C.S., and Kim, W.U. (2017). Transcription factor NFAT5 promotes macrophage survival in rheumatoid arthritis. J. Clin. Invest. *127*, 954–969.

Christian, F., Smith, E.L., and Carmody, R.J. (2016). The regulation of NF-kappaB subunits by phosphorylation. Cells Basel *5*, 12.

Chrobak, P., Charlebois, R., Rejtar, P., El, B.R., Allard, B., and Stagg, J. (2015). CD73 plays a protective role in collagen-induced arthritis. J. Immunol. *194*, 2487–2492.

Druey, K.M. (2017). Emerging roles of regulators of G protein signaling (RGS) proteins in the immune system. Adv. Immunol. *136*, 315–351.

Fujino, H., and Regan, J.W. (2006). EP(4) prostanoid receptor coupling to a pertussis toxin-sensitive inhibitory G protein. Mol. Pharmacol. *69*, 5–10.

Funk, C.D. (2001). Prostaglandins and leukotrienes: advances in eicosanoid biology. Science *294*, 1871–1875.

Gasparini, C., and Feldmann, M. (2012). NF-kappaB as a target for modulating inflammatory responses. Curr. Pharm. Des. *18*, 5735–5745.

Gavalda, N., Gutierrez, H., and Davies, A.M. (2009). Developmental switch in NF-kappaB signalling required for neurite growth. Development *136*, 3405–3412.

Goulet, J.L., Pace, A.J., Key, M.L., Byrum, R.S., Nguyen, M., Tilley, S.L., Morham, S.G., Langenbach, R., Stock, J.L., McNeish, J.D., et al. (2004). E-prostanoid-3 receptors mediate the proinflammatory actions of prostaglandin E2 in acute cutaneous inflammation. J. Immunol. *173*, 1321–1326.

Huang, J., Chen, L., Yao, Y., Tang, C., Ding, J., Fu, C., Li, H., and Ma, G. (2016). Pivotal role of regulator of G-protein signaling 12 in pathological cardiac hypertrophy. Hypertension *67*, 1228–1236.

Inglis, J.J., Criado, G., Medghalchi, M., Andrews, M., Sandison, A., Feldmann, M., and Williams, R.O. (2007). Collagen-induced arthritis in C57BL/6 mice is associated with a robust and sustained T-cell response to type II collagen. Arthritis Res. Ther. *9*, R113.

Kang, J.L., Jung, H.J., Lee, K., and Kim, H.R. (2006). Src tyrosine kinases mediate crystalline silica-induced NF-kappaB activation through tyrosine phosphorylation of IkappaB-alpha and p65 NF-kappaB in RAW 264.7 macrophages. Toxicol. Sci. *90*, 470–477.

Kimple, R.J., De Vries, L., Tronchere, H., Behe, C.I., Morris, R.A., Gist, F.M., and Siderovski, D.P. (2001). RGS12 and RGS14 GoLoco motifs are G alpha(i) interaction sites with guanine nucleotide dissociation inhibitor activity. J. Biol. Chem. *276*, 29275–29281.

Liu, T., Zhang, L., Joo, D., and Sun, S.C. (2017). NF-kappaB signaling in inflammation. Signal. Transduct. Target Ther. *2*, 17023.

Matsumoto, I., Staub, A., Benoist, C., and Mathis, D. (1999). Arthritis provoked by linked T and B cell recognition of a glycolytic enzyme. Science *286*, 1732–1735.

Milanovic, M., Kracht, M., and Schmitz, M.L. (2014). The cytokine-induced conformational switch of nuclear factor kappaB p65 is mediated by p65 phosphorylation. Biochem. J. *457*, 401–413.

Neubig, R.R., and Siderovski, D.P. (2002). Regulators of G-protein signalling as new central nervous system drug targets. Nat. Rev. Drug Discov. *1*, 187–197.

Park, J.S., Kim, S.H., Kim, K., Jin, C.H., Choi, K.Y., Jang, J., Choi, Y., Gwon, A.R., Baik, S.H., Yun, U.J.,

et al. (2015). Inhibition of notch signalling ameliorates experimental inflammatory arthritis. Ann. Rheum. Dis. *74*, 267–274.

Patel, J., McNeill, E., Douglas, G., Hale, A.B., de Bono, J., Lee, R., Iqbal, A.J., Regan-Komito, D., Stylianou, E., Greaves, D.R., et al. (2015). RGS1 regulates myeloid cell accumulation in atherosclerosis and aortic aneurysm rupture through altered chemokine signalling. Nat. Commun. *6*, 6614.

Ponting, C.P. (1999). Raf-like Ras/Rap-binding domains in RGS12- and still-life-like signalling proteins. J. Mol. Med. (Berl) *77*, 695–698.

Pope, R.M. (2002). Apoptosis as a therapeutic tool in rheumatoid arthritis. Nat. Rev. Immunol. *2*, 527–535.

Qi, H., Zhang, Y.B., Sun, L., Chen, C., Xu, B., Xu, F., Liu, J.W., Liu, J.C., Chen, C., Jiao, W.W., et al. (2017). Discovery of susceptibility loci associated with tuberculosis in Han Chinese. Hum. Mol. Genet. *26*, 4752–4763.

Rao, J.S., Langenbach, R., and Bosetti, F. (2005). Down-regulation of brain nuclear factor-kappa B pathway in the cyclooxygenase-2 knockout mouse. Brain Res. Mol. Brain Res. *139*, 217–224.

Sack, U., Stiehl, P., and Geiler, G. (1994). Distribution of macrophages in rheumatoid synovial membrane and its association with basic activity. Rheumatol. Int. *13*, 181–186.

Samad, T.A., Moore, K.A., Sapirstein, A., Billet, S., Allchorne, A., Poole, S., Bonventre, J.V., and Woolf, C.J. (2001). Interleukin-1beta-mediated induction of Cox-2 in the CNS contributes to inflammatory pain hypersensitivity. Nature *410*, 471–475.

Schiff, M.L., Siderovski, D.P., Jordan, J.D., Brothers, G., Snow, B., De Vries, L., Ortiz, D.F., and Diverse-Pierluissi, M. (2000). Tyrosine-kinase-dependent recruitment of RGS12 to the N-type calcium channel. Nature *408*, 723–727.

Schroer, A.B., Mohamed, J.S., Willard, M.D., Setola, V., Oestreich, E., and Siderovski, D.P. (2019). A role for regulator of G protein Signaling-12 (RGS12) in the balance between myoblast proliferation and differentiation. PLoS One *14*, e216167.

Siderovski, D.P., Diverse-Pierluissi, M., and De Vries, L. (1999). The GoLoco motif: a Galphai/o binding motif and potential guanine-nucleotide exchange factor. Trends. Biochem. Sci. *24*, 340–341.

Smolen, J.S., Aletaha, D., and McInnes, I.B. (2016). Rheumatoid arthritis. Lancet *388*, 2023–2038.

Snow, B.E., Antonio, L., Suggs, S., Gutstein, H.B., and Siderovski, D.P. (1997). Molecular cloning and expression analysis of rat Rgs12 and Rgs14. Biochem. Biophys. Res. Commun. *233*, 770–777.

Snow, B.E., Hall, R.A., Krumins, A.M., Brothers, G.M., Bouchard, D., Brothers, C.A., Chung, S., Mangion, J., Gilman, A.G., Lefkowitz, R.J., et al. (1998). GTPase activating specificity of RGS12 and binding specificity of an alternatively spliced PDZ (PSD-95/Dlg/ZO-1) domain. J. Biol. Chem. *273*, 17749–17755.

Sprague, A.H., and Khalil, R.A. (2009). Inflammatory cytokines in vascular dysfunction and vascular disease. Biochem. Pharmacol. *78*, 539–552.

Sundaram, K., Senn, J., Yuvaraj, S., Rao, D.S., and Reddy, S.V. (2009). FGF-2 stimulation of RANK ligand expression in Paget's disease of bone. Mol. Endocrinol. *23*, 1445–1454.

Tang, W., Lu, Y., Tian, Q.Y., Zhang, Y., Guo, F.J., Liu, G.Y., Syed, N.M., Lai, Y., Lin, E.A., Kong, L., et al. (2011). The growth factor progranulin binds to TNF receptors and is therapeutic against inflammatory arthritis in mice. Science *332*, 478–484.

Tipton, D.A., Gay, D.C., and DeCoster, V.A. (2007). Effect of a cyclooxygenase-2 inhibitor on interleukin-1beta-stimulated activation of the transcription factor nuclear factor-kappa B in human gingival fibroblasts. J. Periodontol. *78*, 542–549.

Uhlik, M.T., Temple, B., Bencharit, S., Kimple, A.J., Siderovski, D.P., and Johnson, G.L. (2005). Structural and evolutionary division of phosphotyrosine binding (PTB) domains. J. Mol. Biol. *345*, 1–20.

Vallabhapurapu, S., and Karin, M. (2009). Regulation and function of NF-kappaB transcription factors in the immune system. Annu. Rev. Immunol. *27*, 693–733.

Willard, M.D., Willard, F.S., Li, X., Cappell, S.D., Snider, W.D., and Siderovski, D.P. (2007). Selective role for RGS12 as a Ras/Raf/MEK scaffold in nerve growth factor-mediated differentiation. EMBO J. *26*, 2029–2040.

Yamamoto, Y., and Gaynor, R.B. (2001). Therapeutic potential of inhibition of the NF-kappaB pathway in the treatment of inflammation and cancer. J. Clin. Invest. *107*, 135–142.

Yang, S., Li, Y.P., Liu, T., He, X., Yuan, X., Li, C., Cao, J., and Kim, Y. (2013). Mx1-cre mediated Rgs12 conditional knockout mice exhibit increased bone mass phenotype. Genesis *51*, 201–209.

Yao, Z., Xing, L., and Boyce, B.F. (2009). NF-kappaB p100 limits TNF-induced bone resorption in mice by a TRAF3-dependent mechanism. J. Clin. Invest. *119*, 3024–3034.

You, S., Yoo, S.A., Choi, S., Kim, J.Y., Park, S.J., Ji, J.D., Kim, T.H., Kim, K.J., Cho, C.S., Hwang, D., et al. (2014). Identification of key regulators for the migration and invasion of rheumatoid synoviocytes through a systems approach. Proc. Natl. Acad. Sci. U S A *111*, 550–555.

Yuan, G., Xu, L., Cai, T., Hua, B., Sun, N., Yan, Z., Lu, C., and Qian, R. (2019). Clock mutant promotes osteoarthritis by inhibiting the acetylation of NFkappaB. Osteoarthritis Cartilage *27*, 922–931.

Yuan, X., Cao, J., Liu, T., Li, Y.P., Scannapieco, F., He, X., Oursler, M.J., Zhang, X., Vacher, J., Li, C., et al. (2015). Regulators of G protein signaling 12 promotes osteoclastogenesis in bone remodeling and pathological bone loss. Cell Death Differ. *22*, 2046–2057.

iScience, Volume *23*

Supplemental Information

RGS12 Is a Novel Critical

NF-κB Activator in Inflammatory Arthritis

Gongsheng Yuan, Shuting Yang, Andrew Ng, Chuanyun Fu, Merry Jo Oursler, Lianping Xing, and Shuying Yang

Supplemental figures and legends

Figure S1.

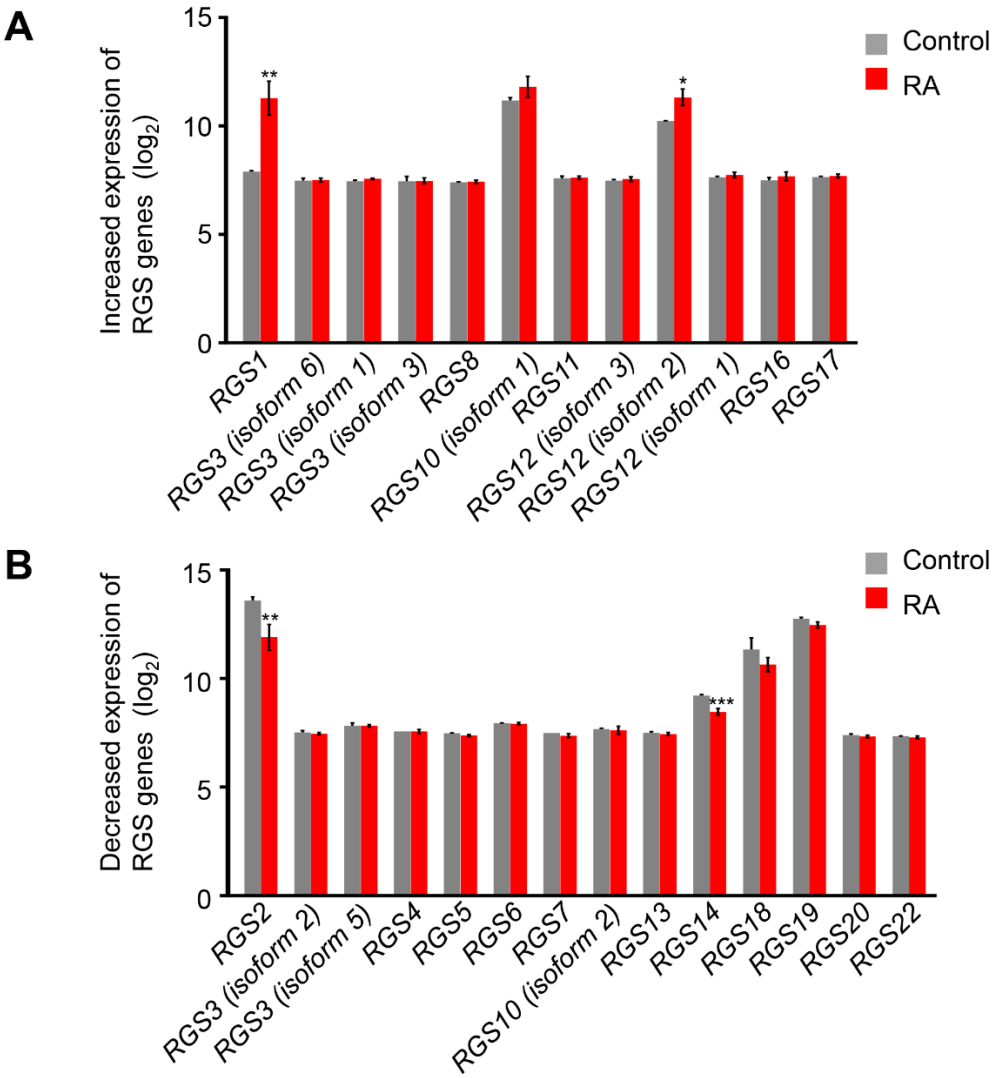

Figure S1. RGS family gene expression in RA macrophages, Related to Figure 1
RNA-seq analysis of control and RA samples from macrophages. (A) Increased expression of RGS genes was exhibited. Of these, *RGS1* and *RGS12 (isoform 2)* genes were significantly increased in RA macrophages. (B) Decreased expression of RGS genes was exhibited. Of these, *RGS2* and *RGS14* genes were significantly decreased in RA macrophages. *p < 0.05. **p <0.01.

Figure S2.

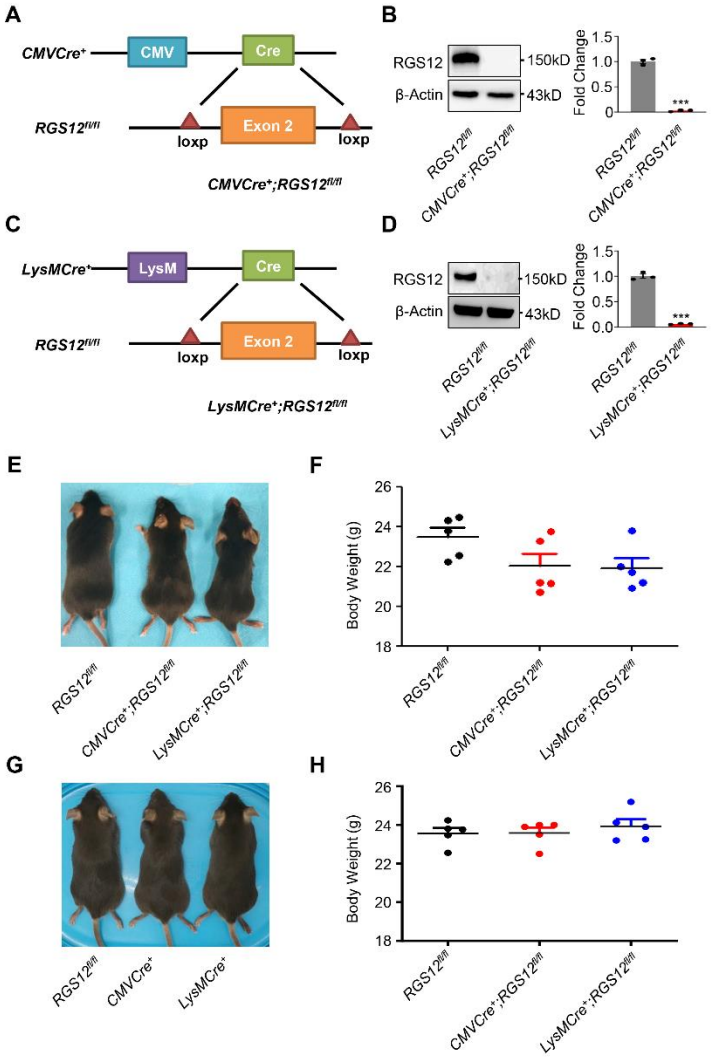

Figure S2. Molecular characterization of RGS12 global and conditional knockout mice, Related to Figure 2

(A) Schematic representation of the *RGS12* gene after exposure to *CMVCre*$^{+}$.

(B) BMMs from *RGS12*$^{fl/fl}$ and *CMVCre*$^{+}$*; RGS12*$^{fl/fl}$ were analyzed by immunoblot assay. ***p < 0.001, (n=3).

(C) Schematic representation of the *RGS12* gene after exposure to *LysMCre*$^{+}$.

(D) BMMs from *RGS12*$^{fl/fl}$ and *CMVCre*$^{+}$*; RGS12*$^{fl/fl}$ were analyzed by immunoblot assay. ***p < 0.001, (n=3).

(E) Appearance of *CMVCre*$^{+}$*;RGS12*$^{fl/fl}$ and *LysMCre*$^{+}$*;RGS12*$^{fl/fl}$ mice.

(F) Body weight of *CMVCre*$^{+}$*;RGS12*$^{fl/fl}$ and *LysMCre*$^{+}$*;RGS12*$^{fl/fl}$ mice. *p < 0.05, (n=5). Note that *CMVCre*$^{+}$*;RGS12*$^{fl/fl}$ and *LysMCre*$^{+}$*;RGS12*$^{fl/fl}$ mice showed mild trend of decrease.

(G) Appearance of *RGS12*$^{fl/fl}$, *CMVCre*$^{+}$ and *LysMCre*$^{+}$ mice.

(H) Body weight of *RGS12*$^{fl/fl}$, *CMVCre*$^{+}$ and *LysMCre*$^{+}$ mice. *p < 0.05, (n=5). Note that there was no significant difference compared with *RGS12*$^{fl/fl}$.

Figure S3.

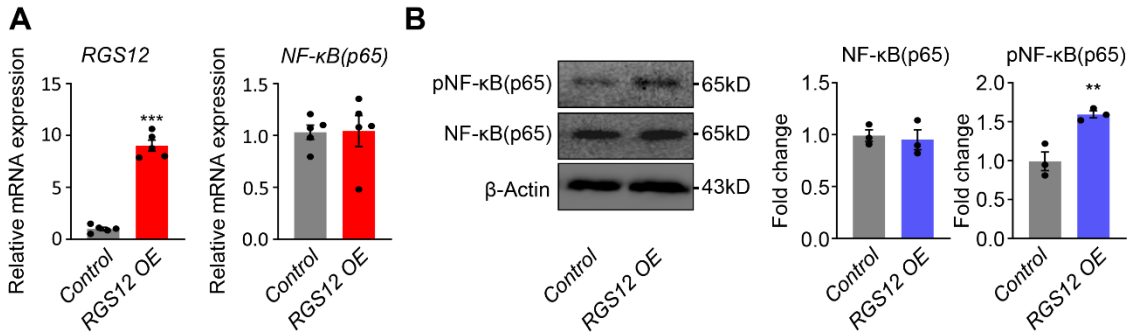

Figure S3. Forced expression of *RGS12* does not affect the total NF-κB(p65) expression, Related to Figure 3

(A) The relative gene expression levels showing that overexpression of RGS12 (*RGS12 OE*, 3μg) in RAW264.7 cells does not affect the *NF-κB(p65)* expression. The t-test showed significant differences between the two groups, ***$p < 0.001$ versus control, n=5.

(B) Immunoblot showed the NF-κB(p65) and phosphorylation levels in RGS12 overexpression (*RGS12 OE*,3μg) RAW264.7 cells. **$p < 0.01$ versus control. Note that overexpression of RGS12 can upregulate the phosphorylation of NF-κB(p65) but not the total NF-κB(p65). Data are representative of 3 separate experiments.

Figure S4.

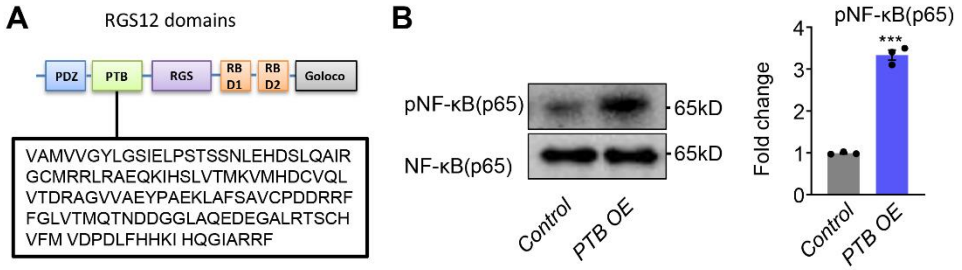

Figure S4. PTB domain of RGS12 promotes the phosphorylation of NF-κB(p65), Related to Figure 4

(A) Schematic representation of the PTB domain of RGS12.

(B) Western blot analysis for the phosphorylation of NF-κB(p65) and the total NF-κB(p65) expression in RAW264.7 cells stably transfected with *RGS12-PTB* domain lentivirus. **$p < 0.01$ versus control. Data are representative of 3 separate experiments.

Figure S5.

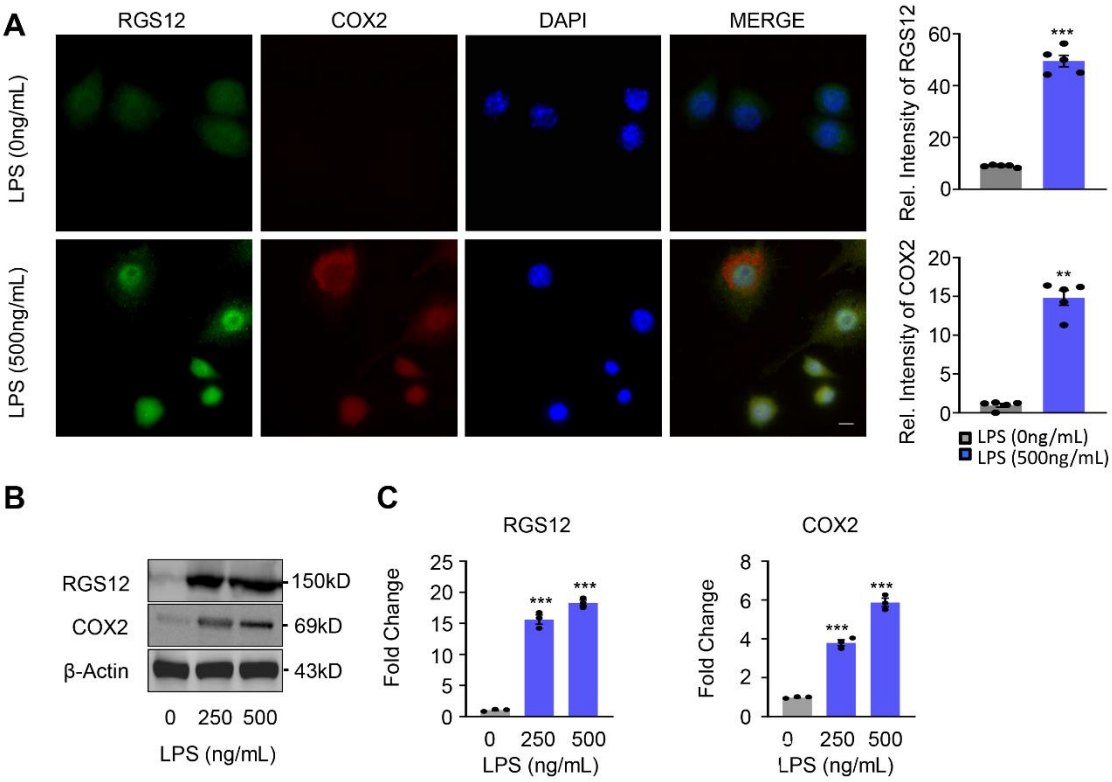

Figure S5. The expression levels of RGS12 and COX2 increase in LPS induced BMMs, Related to Figure 5

(A) Immunofluorescence staining for RGS12 and COX2 expression in BMMs treated with different doses of LPS (0 and 500 ng/mL). Quantification of RGS12 expression, measured by the ImageJ densitometry method. ***p < 0.001 and **p < 0.01versus control. Note that RGS12 and COX2 increase in LPS induced cells.

(B) Immunoblot analysis for the expression of RGS12 and COX2 in the different doses of LPS (0, 250 and 500 ng/mL) induced BMMS.

(C) Quantification of immunoblot shows RGS12 and COX2 increase in LPS induced BMMs. **p < 0.01, ***p < 0.001 versus the control group. Data are representative of 3 separate experiments.

Figure S6.

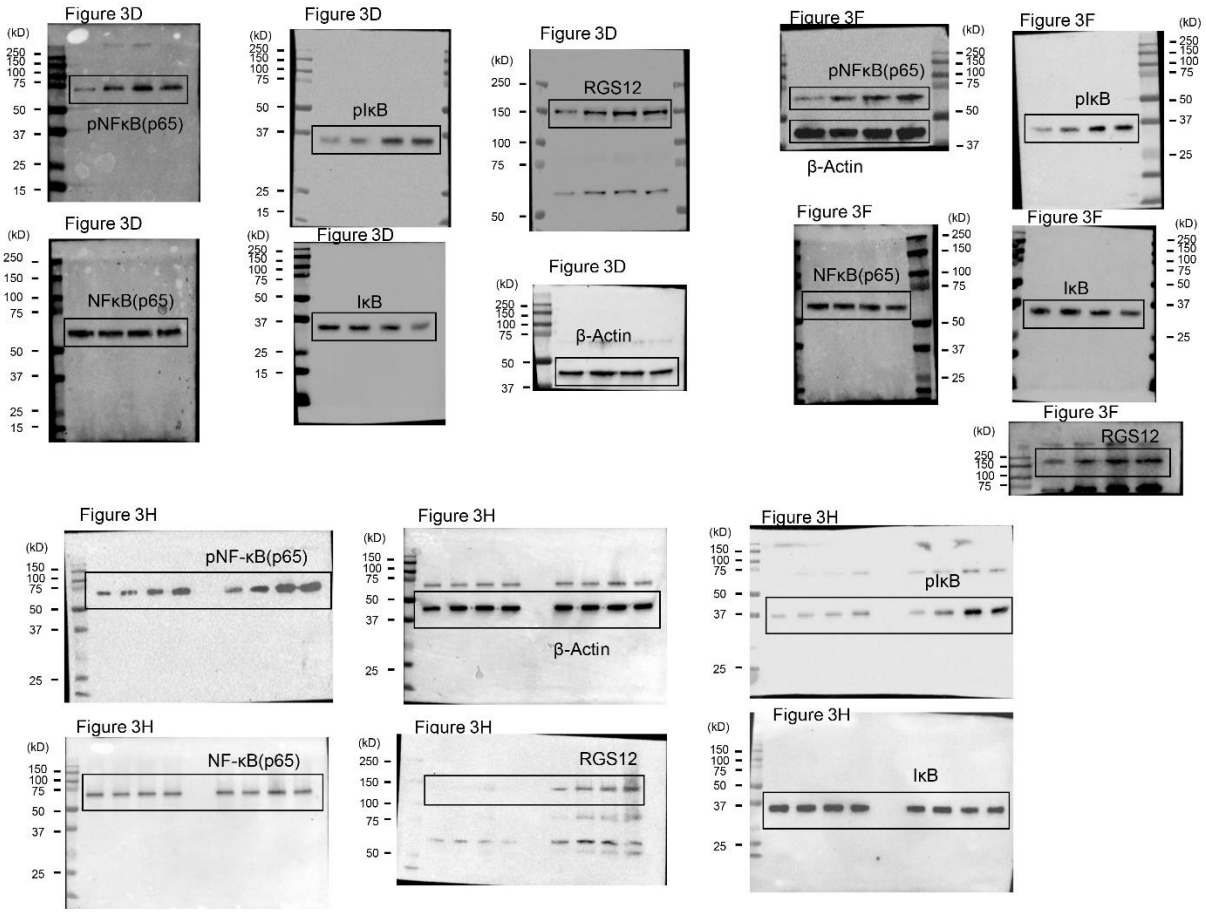

Figure S6. Uncropped scans with size marker indications, Related to Figure 3

Supplemental Tables

Table S1 Evaluation for clinical arthritis, Related to Figure 2

Score	Description
0	No pathological changes
1	Mild swelling confined to the tarsal bones or ankle joint
2	Swelling or erythema extending from the ankle to the tarsal bones
3	Moderate swelling extending from the ankle to the metatarsal joints
4	Severe swelling encompassing the ankle or ankylosis of the limb

Table S2 Synovial pathology scoring, Related to Figure 2

Score	Description
0	No pathological changes
1	Minimal multifocal small (no measurable aggregates) subsynovial accumulations of inflammatory cells
2	Diffuse small (no measurable aggregates) subsynovial accumulations of inflammatory cells
3	Diffuse small subsynovial accumulations of inflammatory cells (1–3 aggregates measuring at least 100 μM in diameter)
4	Diffuse small subsynovial accumulations of inflammatory cells (>3 aggregates measuring at least 100 μM in diameter)
5	Diffuse severe inflammation with numerous aggregates

Table S3 Mouse Primers Used for PCR Analysis, Related to Figure 1 and Figure 5

Gene		Primer Sequence	Ta(ºC)
RGS12(m)	Forward	CAGAGTACCCTGCCGAGAAG	60
	Reverse	AGTCTGGGTCCACCATGAAC	
RGS12(h) iso1	Forward	ATGTTTAGAGCTGGGGAGGCCT	
	Reverse	GACGAAGGTGGCGTGGTGA	
RGS12(h) iso2	Forward	ATGTTTAGAGCTGGGGAGGCCT	60
	Reverse	GAACCTGGAGGTACCTGGTCTG	
RGS12(h) iso3	Forward	TGGCTCGGTGCCTTACAATGA	60
	Reverse	AGCTCAGACGAAGGTGGCGT	
NF-κB	Forward	GGCCTCATCCACATGAACTT	60
	Reverse	CACTGTCACCTGGAAGCAGA	
IL1	Forward	GCCCATCCTCTGTGACTCAT	60
	Reverse	AGGCCACAGGTATTTTGTCG	
IL6	Forward	AGTTGCCTTCTTGGGACTGA	60
	Reverse	TCCACGATTTCCCAGAGAAC	
TNFα	Forward	CGTCAGCCGATTTGCTATCT	60
	Reverse	CGGACTCCGCAAAGTCTAAG	
COX2	Forward	AGAAGGAAATGGCTGCAGAA	60
	Reverse	GCTCGGCTTCCAGTATTGAG	

Chip-1 *RGS12*	Forward	TGTGTACATGTTTGTGTGTGCTC	60
	Reverse	GGCAAGGTAATGCAGCCTAA	
Chip-2 *RGS12*	Forward	TGTGTACATGTTTGTGTGTGCTC	60
	Reverse	TAATTCCTGTACTGTGGAAAGAGA	
GAPDH	Forward	AGGTCGGTGTGAACGGATTTG	60
	Reverse	TGTAGACCATGTAGTTGAGGTCA	

Table S4 Demographics for RA Patients, Related to Figure 1

Subject ID	Age	Gender	Background
S06-000497	80 YR	F	Inflamed synovial tissue with RA.
S06-002876	76 YR	F	Consistent with rheumatoid nodules.
S06-008182	71 YR	F	Moderate chronic synovitis with RA.
S06-008965	29 YR	F	Benign fibrous tissue with RA.
S07-012295	69 YR	M	Fibromembranous tissue with RA
S07-020179	38 YR	M	Consistent with rheumatoid nodule.
S07-020180	70 YR	F	Consistent with rheumatoid nodule.
S07-023846	61 YR	F	Consistent with rheumatoid nodule.
S07-024582	64 YR	M	Features compatible with a rheumatoid nodule.

Transparent Methods

In vivo animal studies

The *RGS12* gene target vector contains 1.1 kb and 4.92 kb of homologous genomic DNA and 4.22kb of excised DNA flanked with LoxP. The 4.22 kb fragment which contains exon 2 (encoding 627 aa that contains both PDZ and PTB domains) of the RGS12 gene was flanked with LoxP and excised. To globally inactivate RGS12, we crossed the *RGS12*$^{fl/fl}$ mice with *CMVCre*$^{+}$ transgenic mice, which express Cre under the cytomegalovirus minimal promoter. To specifically inactivate RGS12 in the myeloid cell lineage (monocytes, mature macrophages, and granulocytes), we crossed the *RGS12*$^{fl/fl}$ mice with *LysMCre*$^{+}$ transgenic mice (also known as B6N.129P2(B6)-Lyz2), which express Cre under the control of the endogenous Lyz2 promoter/enhancer elements. The Cre transgene was detected using two primers Cre-F (CCTGGAAAATGCTTCT GTCCGTTTGCC) and Cre-B (GGCGCGGCAACACCATTTTT). The floxed and wild-type alleles were genotyped by two primers: RGS12-S (CAGTTATTGGAAACTATCTCATGAC); and RGS12-W (CACCGCACACACACAAAATAAATATCA), which yielded a 385bp band for the flox allele and a 260bp band for wild-type allele. Genotyping of mice was performed by PCR using proteinase K-digested tail DNA.

Female mice, of the *RGS12*$^{fl/fl}$ mice and age-matched *CMVCre*$^{+}$*; RGS12*$^{fl/fl}$ and *LysMCre*$^{+}$*; RGS12*$^{fl/fl}$ mice, were used at an age of 8-12 weeks and bred in the University Laboratory Animal Resources (ULAR) of University of Pennsylvania. All animal studies were performed in accordance with institutional guidelines and with

approval by the Institutional Animal Care and Use Committee of the University of Pennsylvania.

Cell culture

BMMs were isolated from the tibia and femur as described in our previous study (Yuan et al., 2015) and cultured for 5 days in DMEM (ThermoFisher Scientific, 11995-073) supplemented with 10% FBS, 5000U/mL M-CSF, non-essential amino acids, sodium pyruvate and 1% penicillin and streptomycin (ThermoFisher Scientific, 15070-063). BMMs in the antibiotic-free medium were seeded onto 12-well plates at a density of 1×10^6 cells per well, followed by incubation overnight.

$F4/80^+$ cells were isolated from synovial fluid by indirect magnetic labeling according to the manufacturer's protocol (ThermoFisher Scientific, 11203D). Briefly, cells were suspended in phosphate-buffered saline (PBS) containing anti-F4/80 antibody for 30 min, then the cells were washed with PBS and mixed with streptavidin-labeled magnetic particles. Labeled cells were subjected to magnetic separation and collected by the addition of DMEM.

RAW 264.7 cells were acquired from the American Type Culture Collection (TIB-71). Cells were maintained in complete growth medium (DMEM supplemented with 2 mM glutamine, 100 units/mL penicillin, 100 mg/mL streptomycin and 10% FBS). Cells were passaged by gently lifting the cells with a disposable cell scraper, pelleting by centrifugation and replanting the cells in fresh complete medium.

Collagen-induced arthritis (CIA) model

8-week-old female *RGS12*$^{fl/fl}$, *CMVCre*$^+$*;RGS12*$^{fl/fl}$ and *LysMCre*$^+$*;RGS12*$^{fl/fl}$ mice (n=5/group) were immunized via a 0.1 mL subcutaneous injection at the base of the tail

with 100 μg chicken type II collagen (Chondrex, LLC, Seattle, WA) emulsified with an equal volume of complete Freund's adjuvant (CFA) containing 4 mg/mL heat-denatured mycobacterium (Chondrex, LLC, Seattle, WA) (day 0). A booster injection of 100 μg chicken type II collagen emulsified with an equal volume of complete Freund adjuvant (Chondrex, LLC, Seattle, WA) was administered on day 21 (Yuan et al., 2014).

Evaluation of clinical arthritis

Clinical manifestations of arthritis were assessed daily on a scale of 0–4 (Table S1) (0, no sign; 1, slight swelling or erythema; 2, swelling or erythema extending from the ankle to the tarsal bones 3, moderate erythema and swelling in multiple digits or entire paw; 4, pronounced erythema and swelling of entire paw or ankylosis of the limb), with a maximum score of 16 (4 score × 4 paws) per mouse. Change from baseline in paw thickness was determined daily by dial calipers, and an average change in ankle thickness was determined for each mouse from the 2 hind paw measurements. On day 40, mice were sacrificed, and mouse blood, paws, and organs were harvested for analysis.

Therapeutic studies of nanoparticle carrying *RGS12 shRNA* in mild RA mouse model

8-week-old female C57BL/6 mice (n=5/group) were immunized via a 0.1 mL subcutaneous injection at the base of the tail as described above for 30 days to create the mild RA mice (clinical score 8-10). Mild RA mice were randomly divided into two groups (n=5) and received local injections of a recombinant *RGS12 short hair RNA* (*shRGS12*) plasmid (*psi-nU6.1-shRGS12*) or of negative control (*psi-nU6.1-shControl*); the appropriate plasmid was injected into both ankle joint cavities every 3 days for 2 weeks. For each injection, 10 μg of *psi-nU6.1-shRGS12* was mixed with 20 μL of a

nanoparticle *in vivo* DNA transfection reagent (Entranster *in vivo*; North Shore, Auckland, New Zealand) according to the manufacturer's protocol and the procedure previously described (Zheng et al., 2015). Mice ankle joints were harvested on day 46.

X-ray imaging

Mice were taken an X-ray exam under anesthesia. Images were interpreted by certified radiologists and blinded to the final pathologic findings. The assessment included peri-articular soft tissue swelling, articular surface smoothness, and joint space narrowness.

Histological assessment

Human samples were obtained through the PrecisionMed, Inc (Solana Beach, California, US). All tissue samples and data are procured developed networks of research experienced specialist physician clinical sites. The inflammation score was assessed by histological examination on a scale of 0–4 (Table S2 and S4).

Mouse ankle joints were exposed by removing the overlying skin and were subsequently excised and decalcified with EDTA 0.5M (pH=8) for 14 days. A transverse cut was made when the bones were fully decalcified and processed for paraffin embedding. Tissues were cut into 8 μm sections and stained with hematoxylin and eosin to assess joint pathology. The degree of synovial hyperplasia, inflammation, and bone destruction in the joints were determined using a standard scoring protocol (1= weak, 2=moderate, and 3=severe). Synovial hyperplasia has been defined as the increased number of fibroblast-like synoviocytes in the lining layer of the synovium. The severity of inflammation was scored according to the extent of inflammatory cell infiltration into the infrapatellar fat pads, joint capsule, and the area adjacent to the periosteal sheath. Bone destruction was scored according to the loss of cartilage matrix,

disruption, and loss of cartilage surface, and the extent and depth of the subchondral bone erosion.

Microarray analysis

Whole-genome microarray data was obtained using accession numbers GSE 49604 at Gene Expression Omnibus (GEO) (You et al., 2014). Gene expression for annotated genes was normalized and analyzed using R package 3.1.2/Bioconductor, and two-way hierarchical clustering was performed using a correlation similarity metric distance. Groups were compared and genes found to be differentially expressed with a corrected p-value of < 0.05 and an absolute fold change of at least 1.5 were used to find regulation of Gene Ontology Biological Processes terms.

Quantitative real-time qPCR analysis

RNAs from mouse synovium or macrophages were isolated using Trizol reagent (Life Technologies, USA) according to the manufacturer's instructions. Then, 1μg of RNA was reversed transcribed into cDNA using the Reverse Transcription Kit (TAKARA, Japan). Real-time PCR was performed with the reaction mixture containing primers, the cDNA template, and SYBR Green PCR Master Mix (Bio-Rad, USA). The sequences of real-time PCR primers are shown in Table S3.

Co-immunoprecipitation (Co-IP)

RAW264.7 cells were transfected with *p3xFLAG-Myc-CMV-26-RGS12*, *pCMV-NF-κB* and *pcDNA-COX2* plasmids, and proteins were lysed in NP-40 buffer supplemented with protein inhibitor cocktail (PIC) and phenylmethylsulfonyl fluoride (Sigma-Aldrich, US). The main methods were performed as described (Yuan et al., 2017). Briefly, the lysates of equal amounts of protein were incubated at room temperature with primary

antibodies for 1 hour and then with protein A/G beads overnight, after which the beads were washed with PBST. Bound proteins were solubilized in loading buffer for Western blot analysis.

Western blot

BMMs or synovium were homogenized with RIPA buffer (50 mM Tris, 150 mM NaCl, 1% Triton X-100,0.1% SDS, and 1% sodium deoxycholate) containing PIC (Sigma-Aldrich, US) on ice. Nuclear and cytoplasmic proteins were extracted using commercial reagents (Nuclear Extraction Kit #2900, Millipore, USA) according to the manufacturer's protocol. Protein concentration was measured using BCA protein assay reagent (Thermo Fisher Scientific). Equal amounts of protein (30μg) were denatured in SDS and separated in 10% SDS–PAGE gels. Proteins were transferred to NC membranes in transfer buffer containing 20% methanol. The membranes were blocked with 5% skim milk, incubated with primary antibody overnight at 4 and then incubated with horseradish peroxidase (HRP)-conjugated second antibody (1:5,000, Jackson ImmunoResearch, PA) at room temperature for 1 h. Signals were analyzed using an ECL Western blotting system (Bio-Rad Laboratories, Hercules, CA, USA). β-Actin (1:3,000, sc-47778 HRP, Santa Cruz) was used as the internal control. The same procurer was used to determine the RGS12 (1:1,000, GW21317, Sigma-Aldrich) , Phospho-NF-κB(p65) (Ser536) (1:1,000, 3033, Cell Signaling Technology), Phospho-IκBα (Ser32) (1:1,000, 2859, Cell Signaling Technology), NF-κB(p65) (1:1,000, 8242, Cell Signaling Technology), IκBα (1:1,000, 4814, Cell Signaling Technology), COX2 (1:1,000, 12282, Cell Signaling Technology), IL6 (1:1,000, 21865-1-AP, Proteintech) and Lamin B (1:1,000, 12987-1-AP, Proteintech).

PGE2 Enzyme-Linked Immunosorbent Assay (ELISA)

High binding ELISA plates were coated with the anti-PGE2 monoclonal antibody in 0.1M carbonate buffer pH 9.5 overnight and blocked with 1x BSA overnight. Samples were then applied to the plates either whole or diluted in the block with 10mM EDTA. The standard curve was prepared using recombinant mouse PGE2 (R&D Systems) in the block with 10mM EDTA. Between steps, plates were washed with PBS plus 0.05% Tween. The plates were visualized with TMB substrate (Thermo Fisher), stopped with 2M H2SO4, and analyzed on a colorimetric plate reader (Microplate Absorbance Reader #1681130, Bio-Rad, USA).

Plasmid construction

Full Length of *RGS12* cDNA fragment (NCBI Reference Sequence: NM_173402.2) was cloned and inserted into the *p3xFLAG-Myc-CMV-26* backbone. Full Length of *COX2* cDNA (also known as *ptgs2*, NM_011198.4) was cloned and inserted into the *pcDNA3.1-C-HA* backbone. *T7-RelA/NF-κB* was a gift from Warner Greene (Addgene plasmid # 21984).

RGS12 mutants were generated and cloned to *p3xFLAG-Myc-CMV-26* vector, respectively, by deleting amino acids 19-95 (PDZ), 227-358 (PTB),716-830 (RGS),963-1035 (RBD1),1035-1104 (RBD2) and 1188-1209 (GoLoco) of the coding region (NCBI Reference Sequence: NP_775578.2).

shRNA and siRNA construction

Non-targeting *RGS12 siRNA* and *RGS12 shRNAs* were obtained from GeneCopoeia, Inc (San Diego, CA). Target sequences were as follows: Control sh/siRNA: GCTTCGCGCCGTAGTCTTA; *RGS12 sh/siRNA 1*: CTAGGCAAGTCTAACTCTATT;

RGS12 sh/siRNA 2: CCTGTCCATGATTAATAAAGG; *RGS12 sh/siRNA 3*: AGTCTGCAACTGTGTCTGATGGCGAGTTG. *NF-κB(p65) shRNA1* and *shRNA2* were gifts from Tyler Jacks (Addgene plasmid # 22507; #22508).

Transfection

RAW264.7 or 293T cell lines were seeded on 6-well plates at 3×10^5 cells/well (approximately 90-95% confluency). Cells were transfected on the following day with FuGENE HD Transfection Reagent (E2311, Promega Corporation). Cells were harvested at 48 hours after transfection.

Virus production and Infection

293T packaging cell lines were used for lentiviral amplification. Lentiviral infection was carried out as previously described (Dyall et al., 2001). Briefly, viruses were collected at 48 h and 72 h post-transfection. After passing through 0.45-μm filters, viruses were used to infect target cells. Subsequently, stable target cell lines underwent appropriate antibiotic selection.

Immunofluorescence (IF)

The frozen sections (8 μm) of harvested paws were fixed in 4% paraformaldehyde for 20 minutes at room temperature, incubated with RGS12 (1:100 dilution; Abcam), NF-κB(p65) (1:200 dilution; Cell Signaling Technology, USA), and COX2 (1:100 dilution; Cell Signaling Technology, USA), followed by incubation with the appropriate secondary antibody (1:100 dilution; Jackson Immunoresearch Laboratory). All images were visualized on a Leica microscope and acquired at the same exposure time with Image J software. The relative intensity of the fluorescence was determined by comparing each intensity value to the average intensity of spread cells.

Chromatin immunoprecipitation (ChIP)

We conducted ChIP assays according to the manufacturer's protocol (Cell Signaling Technologies, 9004S) (Yuan et al., 2017). Brief, cells were cross-linked with 1% formaldehyde for 10 min at room temperature and quenched with glycine to a final concentration of 0.125 M for another 5 min. Chromatin was incubated with micrococcal nuclease for 20 min at 37°C and sonicated with a Bioruptor, and incubated overnight at 4 °C with 5 μg of the desired antibodies: NF-κB(p65) (8242, Cell Signaling Technology, USA) and IgG (53484, Cell Signaling Technology, USA). Immunocomplexes were immobilized with 100 μL of protein-G Dynal magnetic beads overnight at 4 °C, followed by stringent washes and elution. Eluates were reverse cross-linked overnight at 65 °C and deproteinated with proteinase K at 56 °C for 30 min. DNA was extracted with phenol-chloroform, followed by ethanol precipitation. ChIP-qPCR signals were calculated as the percentage of input. The sequences of ChIP primers are shown in Table S3.

Luciferase Assays

Luciferase assays were performed according to the procedure described previously (Yuan et al., 2017). The *pLightSwitch-RGS12* plasmid was constructed by cloning human *RGS12* promoter (-2000bp) to *pLightSwitch* vector (S790005, SwitchGear Genomics, USA). Then, 1 μg of *pLightSwitch-RGS12* plasmid, 1 μg of *pLightSwitch control* plasmid and 1-5 μg of *NF-κB(p65)* plasmids were co-transfected into HEK293T cells in 6-well plates by using Lipofectamine 2000 reagent (11668, Thermo Fisher Scientific). Cells were harvested 48 hours after transfection, and then firefly and renilla

luciferase activity were detected by using the dual-luciferase reporter gene assay kit (Progema, USA).

Statistical Analysis

The data from the experiments were analyzed by several statistical methods. Error bars represent the SEM, and statistical significance was determined by unpaired two-tailed Student t-test; An analysis of variance test was first performed to compare the mean values between groups, and the Student–Newman–Keuls test was used to compare the mean values between two conditions with the GraphPad software. In all cases, P values less than 0.05 were considered significant.

Supplemental References

Dyall, J., Latouche, J.B., Schnell, S., and Sadelain, M. (2001). Lentivirus-transduced human monocyte-derived dendritic cells efficiently stimulate antigen-specific cytotoxic T lymphocytes. BLOOD *97*, 114-121.

You, S., Yoo, S.A., Choi, S., Kim, J.Y., Park, S.J., Ji, J.D., Kim, T.H., Kim, K.J., Cho, C.S., and Hwang, D., et al. (2014). Identification of key regulators for the migration and invasion of rheumatoid synoviocytes through a systems approach. Proc Natl Acad Sci U S A 111, 550-555.

Yuan, G., Hua, B., Yang, Y., Xu, L., Cai, T., Sun, N., Yan, Z., Lu, C., and Qian, R. (2017). The Circadian Gene Clock Regulates Bone Formation Via PDIA3. J BONE MINER RES 32, 861-871.

Yuan, X., Garrett-Sinha, L.A., Sarkar, D., and Yang, S. (2014). Deletion of IFT20 in early stage T lymphocyte differentiation inhibits the development of collagen-induced arthritis. BONE RES 2, 14038.

Zheng, X., Cheng, M., Fu, B., Fan, X., Wang, Q., Yu, X., Sun, R., Tian, Z., and Wei, H. (2015). Targeting LUNX inhibits non-small cell lung cancer growth and metastasis. CANCER RES 75, 1080-1090.